SIAM J. APPL. MATH.
Vol. 64, No. 5, pp. 1810–1838

TIME REVERSAL FOR DISPERSIVE WAVES IN RANDOM MEDIA*

JEAN-PIERRE FOUQUE†, JOSSELIN GARNIER‡, AND ANDRÉ NACHBIN§

Abstract. Refocusing for time reversed waves propagating in disordered media has recently been observed experimentally and studied mathematically. This surprising effect has many potential applications in domains such as medical imaging, underwater acoustics, and wireless communications. Time refocusing for one-dimensional acoustic waves is now mathematically well understood. In this paper the important case of one-dimensional dispersive waves is addressed. Time reversal is studied in reflection and in transmission. In both cases we derive the self-averaging properties of time reversed refocused pulses. An asymptotic analysis allows us to derive a precise description of the combined effects of randomness and dispersion. In particular, we study an important regime in transmission, where the coherent front wave is destroyed while time reversal of the incoherent transmitted wave still enables refocusing.

Key words. dispersive waves, inhomogeneous media, asymptotic theory, time reversal

AMS subject classifications. 76B15, 35Q99, 60F05

DOI. 10.1137/S0036139903422371

1. Introduction.

Time reversal for ultrasound has been extensively studied by Fink and his collaborators at the "Laboratoire Ondes et Acoustique" in Paris; for a description of these experiments we refer, for instance, to the papers [11, 12]. A time reversal mirror is, roughly speaking, a device which is capable of receiving an acoustic signal in time, keeping it in memory, and sending it back into the medium in the reversed direction of time. Time reversal refocusing properties are well understood mathematically for one-dimensional acoustic waves propagating in random media [9] and for three-dimensional waves in layered media [16] or in the paraxial regime [3, 6, 23, 5, 4].

In this paper we consider a case of dispersive waves, namely the Boussinesq model derived in [20]. We first revisit time reversal for reflected signals generated by a pulse sent in a random half-space. The main property of time reversal is the refocusing of the pulse with a shape that depends only on the statistical properties of the medium, and not on the particular realization. This has been mathematically studied in the high-frequency regime for acoustic waves in [9]. We extend this result to the case of dispersive waves. In Theorem 6.1 we derive the deterministic shape of the refocused pulse, which depends on the statistical properties of the medium and the strength of the dispersion. This result is obtained in the regime of weak fluctuations of the medium, a correlation length of the order of magnitude of the pulse carrier wavelength, and long distances of propagation. The underlying asymptotic analysis is based on the techniques of separation of scales presented, for instance, in [2]. In particular, we generalize the system of transport equations that characterize the multiple scattering of the wave.

*Received by the editors February 5, 2003; accepted for publication (in revised form) December 3, 2003; published electronically July 23, 2004. This work was supported by ONR grant N00014-02-1-0089 while the second and third authors were visiting NC State University.

http://www.siam.org/journals/siap/64-5/42237.html

†Department of Mathematics, North Carolina State University, Raleigh NC 27695-8205 (fouque@math.ncsu.edu).

‡Laboratoire de Statistique et Probabilités, Université Paul Sabatier, 118 Route de Narbonne, 31062 Toulouse Cedex 4, France (garnier@cict.fr). This author was supported by program ACI-NIM-2003-94.

§Instituto de Matemática Pura e Aplicada, Est. D. Castorina 110, Jardim Botânico, Rio de Janeiro, RJ 22460-320, Brazil (nachbin@impa.br).

Time reversal refocusing can also be obtained from transmitted waves generated by a pulse propagating through a slab of random medium. For dispersive waves, in contrast with acoustic waves, there is an interesting regime where the coherent front wave is destroyed. We show in this paper that by time reversing the incoherent part of the transmitted wave it is still possible to refocus at the source. We provide a precise analysis of the interplay between randomness and dispersion. In particular, Theorem 7.1 gives the precise description of the refocused pulse.

One potential application discussed in this paper is the characterization by waveform inversion for water waves of the initial sea surface displacement due to tsunamigenic earthquakes [24]. In [24] an adjoint method is proposed. In the synthetic numerical experiments presented there, a shallow water system in two space dimensions is used for the forward propagation, while a linear adjoint method is adopted for the backward identification of the tsunami source. The authors claim that, in principle, the adjoint method can be applied to nonlinear hydrodynamic models. Their method is also applied to real tide gauge series for the small Gorringe Tsunami of 1969, indicating improvements over previous methods. Here we consider a one-dimensional dispersive system, which is valid for longer propagation distances than the hyperbolic shallow water system. Recently we have produced the first analysis for the time reversal of a nonlinear, one-dimensional hyperbolic shallow water system [13]. In particular, we have shown how randomness dramatically improves time reversal experiments. In [13] we have shown that in the presence of randomness one can perform time reversal beyond the shock propagation distance. Randomness acts as an apparent viscosity and regularizes the shock. Extension to linear hyperbolic systems in higher dimensions has been accomplished, for example, in [16]. Hence time reversal for more realistic models in higher dimensions is a promising technique.

Another important fact, regarding applications, is that we have accomplished a mathematical theory for both the time reversal of dispersive waves (the present paper) and also for weakly nonlinear hyperbolic waves [13]. These two papers are important steps in obtaining a mathematical theory for the time reversal of weakly dispersive weakly nonlinear waves, namely solitary waves. This might have a great impact on other models supporting solitons. As a consequence of these two papers, numerical experiments were performed for the time reversal of solitary waves [14].

The paper is organized as follows. In section 2 we introduce the Boussinesq equation including randomness and dispersion, and we describe the different scales arising in the problem. In section 3 we show how the wave can be decomposed into left- and right-propagating modes in the dispersive nonrandom case. This decomposition is crucial in the following sections where the analysis of the random case is performed. In section 4 we establish the system satisfied by the right- and left-going waves in the random case. We also give the integral representation of the transmitted and reflected waves in terms of the mode transmission and reflection coefficients. In section 5 we introduce the time reversal procedures in reflection (TRR) and in transmission (TRT) and derive the corresponding integral representations for the time reversed waves. The two subsequent sections are devoted to the asymptotic analysis of the refocused pulses and comparisons with numerical simulations.

2. The terrain-following Boussinesq model. We consider the Boussinesq equation that describes the evolution of surface waves in shallow channels [20]:

$$M(z)\frac{\partial \eta}{\partial t} + \frac{\partial u}{\partial z} = 0, \tag{2.1}$$

$$\frac{\partial u}{\partial t} + \frac{\partial \eta}{\partial z} - \beta \frac{\partial^3 u}{\partial z^2 \partial t} = 0, \tag{2.2}$$

where η is the wave elevation, u is the depth-averaged velocity, and z and t are the space and time coordinates, respectively. The spatial variations of the coefficient M are imposed by the bottom profile

$$M(z) = 1 + \varepsilon m(z),$$

where 1 stands for the constant mean depth and the dimensionless small parameter ε characterizes the size of the relative fluctuations of the bottom modeled by the zero-mean stationary random process $m(z)$. The process m is assumed to be bounded by a deterministic constant, differentiable, and to have strong mixing properties, such as a rapidly decaying function [22]. We may think, for instance, that $m(z) = f(\nu(z))$, where f is a smooth bounded function and ν is a stationary Gaussian process with Gaussian autocorrelation function and we assume that $\mathbb{E}[f(\nu(0))] = 0$. Note that in that case the realizations of the process ν are of class $\mathcal{C}^\infty$ almost surely. This hypothesis is consistent with the terrain-following coordinate system adopted in deriving (2.1)–(2.2) [20].

We consider the problem on the finite slab $-L \le z \le 0$, where boundary conditions will be imposed at $-L$ and 0 corresponding to a pulse entering the slab from the right at $z = 0$. The quantities of interest, the transmitted and reflected waves, will be observed in time at the extremities $z = -L$ and $z = 0$, respectively.

The coefficient β measures the dispersion strength. In this paper we consider the case where the dispersion parameter β is either of order 1 or small. We consider a pulse whose support is comparable to the correlation length of the random medium, that is, of order 1. In order to see the effect of the small random fluctuations, we consider a long distance of propagation. As we shall see, the interesting regime arises when the propagation distance is of order $1/\varepsilon^2$.

3. The propagating modes of the homogeneous Boussinesq equation. Consider the homogeneous Boussinesq equation (with $m \equiv 0$):

$$\frac{\partial \eta}{\partial t} + \frac{\partial u}{\partial z} = 0, \tag{3.1}$$

$$\frac{\partial u}{\partial t} + \frac{\partial \eta}{\partial z} - \beta \frac{\partial^3 u}{\partial z^2 \partial t} = 0, \tag{3.2}$$

with a smooth initial condition

$$u(t = 0, z) = u_0(z), \qquad \eta(t = 0, z) = \eta_0(z).$$

Taking the space Fourier transform

$$\check{u}(t, k) = \frac{1}{2\pi} \int u(t, z) \exp(ikz) dz, \qquad \check{\eta}(t, k) = \frac{1}{2\pi} \int \eta(t, z) \exp(ikz) dz,$$

the Boussinesq equation (3.1)–(3.2) reduces to a set of ordinary differential equations:

$$\frac{\partial \check{\eta}}{\partial t} = ik\check{u}, \tag{3.3}$$

$$\left(1 + \beta k^2\right) \frac{\partial \check{u}}{\partial t} = ik\check{\eta}. \tag{3.4}$$

Introducing the pulsation corresponding to the wavenumber k through the *dispersion relation*

$$\omega(k) = \frac{k}{\sqrt{1+\beta k^2}}, \tag{3.5}$$

we get closed form expressions for the solutions:

$$\begin{aligned}
\check{u}(t,k) &= \frac{1}{2}\left(\check{u}_0(k) + \frac{\omega}{k}\check{\eta}_0(k)\right)\exp(i\omega t) + \frac{1}{2}\left(\check{u}_0(k) - \frac{\omega}{k}\check{\eta}_0(k)\right)\exp(-i\omega t),\\
\check{\eta}(t,k) &= \frac{1}{2}\left(\frac{k}{\omega}\check{u}_0(k) + \check{\eta}_0(k)\right)\exp(i\omega t) - \frac{1}{2}\left(\frac{k}{\omega}\check{u}_0(k) - \check{\eta}_0(k)\right)\exp(-i\omega t).
\end{aligned}$$

From these expressions we can conclude that any solution can be decomposed as the superposition of left-propagating modes $(u^{(l)}, \eta^{(l)})$ and right-propagating modes $(u^{(r)}, \eta^{(r)})$:

$$\begin{aligned}
u(t,z) &= u^{(r)}(t,z) + u^{(l)}(t,z),\\
\eta(t,z) &= \eta^{(r)}(t,z) + \eta^{(l)}(t,z),
\end{aligned}$$

where

$$\begin{aligned}
u^{(r)}(t,z) &= \int \frac{1}{2}\left(\check{u}_0(k) + \frac{\omega}{k}\check{\eta}_0(k)\right)\exp\left(i\omega(k)t - ikz\right)dk,\\
\eta^{(r)}(t,z) &= \int \frac{k}{2\omega}\left(\check{u}_0(k) + \frac{\omega}{k}\check{\eta}_0(k)\right)\exp\left(i\omega(k)t - ikz\right)dk,\\
u^{(l)}(t,z) &= \int \frac{1}{2}\left(\check{u}_0(k) - \frac{\omega}{k}\check{\eta}_0(k)\right)\exp\left(-i\omega(k)t - ikz\right)dk,\\
\eta^{(l)}(t,z) &= -\int \frac{k}{2\omega}\left(\check{u}_0(k) - \frac{\omega}{k}\check{\eta}_0(k)\right)\exp\left(-i\omega(k)t - ikz\right)dk.
\end{aligned}$$

This decomposition will be used in the nonhomogeneous case in the next section. In [18] a hyperbolic mode decomposition was used as an approximation for the right- and left-propagating modes. Here the mode decomposition is exact for dispersive waves.

4. Propagator formulation. In this section we first express the scattering problem as a two-point boundary value problem in the frequency domain, and then rewrite it as an initial value problem in terms of the propagator. This is the standard approach for acoustic equations [2] that we generalize to the dispersive case using the decomposition introduced in the previous section.

4.1. Mode propagation in the frequency domain. We consider the random Boussinesq equation (2.1)–(2.2) and take the time Fourier transform

$$\hat{u}(\omega,z) = \frac{1}{2\pi}\int u(t,z)\exp(-i\omega t)dt, \qquad \hat{\eta}(\omega,z) = \frac{1}{2\pi}\int \eta(t,z)\exp(-i\omega t)dt,$$

so that the system reduces to a set of ordinary differential equations:

$$\left(1 - \beta\omega^2(1+\varepsilon m(z))\right)\frac{\partial\hat{\eta}}{\partial z} + i\omega\hat{u} - \varepsilon\beta\omega^2 m'(z)\hat{\eta} = 0, \tag{4.1}$$

$$\frac{\partial\hat{u}}{\partial z} + i\omega\left(1+\varepsilon m(z)\right)\hat{\eta} = 0, \tag{4.2}$$

where m' stands for the spatial derivative of m. We introduce the wavenumber k corresponding to the pulsation ω,

$$k(\omega) = \frac{\omega}{\sqrt{1-\beta\omega^2}}, \tag{4.3}$$

so that we can decompose the wave into *right-going modes* A^ε and *left-going modes* B^ε over distances of propagation of order $1/\varepsilon^2$. We show explicitly the dependence on the small parameter ε:

$$A^\varepsilon(\omega,z) = \frac{1}{2}\left(\hat\eta\left(\omega,\frac{z}{\varepsilon^2}\right) + \frac{k}{\omega}\hat u\left(\omega,\frac{z}{\varepsilon^2}\right)\right), \tag{4.4}$$

$$B^\varepsilon(\omega,z) = \frac{1}{2}\left(\hat\eta\left(\omega,\frac{z}{\varepsilon^2}\right) - \frac{k}{\omega}\hat u\left(\omega,\frac{z}{\varepsilon^2}\right)\right). \tag{4.5}$$

The modes $(A^\varepsilon, B^\varepsilon)$ satisfy

$$\begin{aligned}\frac{\partial A^\varepsilon}{\partial z} &= -\frac{ik}{\varepsilon^2}A^\varepsilon - \frac{ik}{2\varepsilon}m\left(\frac{z}{\varepsilon^2}\right)(A^\varepsilon+B^\varepsilon) + \frac{\beta k^2}{2\varepsilon}m'\left(\frac{z}{\varepsilon^2}\right)(A^\varepsilon+B^\varepsilon)\\ &\quad - \frac{i\omega^2}{2k\varepsilon^2}\left(\frac{1}{1-\beta\omega^2(1+\varepsilon m(z/\varepsilon^2))} - \frac{1}{1-\beta\omega^2}\right)(A^\varepsilon - B^\varepsilon)\\ &\quad + \frac{\beta\omega^2}{2\varepsilon}m'\left(\frac{z}{\varepsilon^2}\right)\left(\frac{1}{1-\beta\omega^2(1+\varepsilon m(z/\varepsilon^2))} - \frac{1}{1-\beta\omega^2}\right)(A^\varepsilon+B^\varepsilon),\end{aligned} \tag{4.6}$$

$$\begin{aligned}\frac{\partial B^\varepsilon}{\partial z} &= \frac{ik}{\varepsilon^2}B^\varepsilon + \frac{ik}{2\varepsilon}m\left(\frac{z}{\varepsilon^2}\right)(A^\varepsilon+B^\varepsilon) + \frac{\beta k^2}{2\varepsilon}m'\left(\frac{z}{\varepsilon^2}\right)(A^\varepsilon+B^\varepsilon)\\ &\quad - \frac{i\omega^2}{2k\varepsilon^2}\left(\frac{1}{1-\beta\omega^2(1+\varepsilon m(z/\varepsilon^2))} - \frac{1}{1-\beta\omega^2}\right)(A^\varepsilon - B^\varepsilon)\\ &\quad + \frac{\beta\omega^2}{2\varepsilon}m'\left(\frac{z}{\varepsilon^2}\right)\left(\frac{1}{1-\beta\omega^2(1+\varepsilon m(z/\varepsilon^2))} - \frac{1}{1-\beta\omega^2}\right)(A^\varepsilon+B^\varepsilon).\end{aligned} \tag{4.7}$$

We expand the last terms of the right-hand sides up to $O(\varepsilon^3)$ terms

$$\frac{\omega^2}{1-\beta\omega^2(1+\varepsilon m(z/\varepsilon^2))} - \frac{\omega^2}{1-\beta\omega^2} = \varepsilon\beta k^4 m\left(\frac{z}{\varepsilon^2}\right) + \varepsilon^2\beta^2k^6m^2\left(\frac{z}{\varepsilon^2}\right) + O(\varepsilon^3), \tag{4.8}$$

where the $O(\varepsilon^3)$ is a term that can be bounded by $\varepsilon^3\beta^3k^8\|m\|_\infty^3/(1-\varepsilon\beta k^2\|m\|_\infty)$. We now look at the waves along the *frequency-dependent modified characteristics* defined by

$$a^\varepsilon(\omega,z) = A^\varepsilon(\omega,z)\exp\left(\frac{ikz}{\varepsilon^2}\right)\exp\left(-\frac{\varepsilon\beta k^2}{2}m\left(\frac{z}{\varepsilon^2}\right) - \frac{\varepsilon^2\beta^2k^4}{4}m\left(\frac{z}{\varepsilon^2}\right)^2\right), \tag{4.9}$$

$$b^\varepsilon(\omega,z) = B^\varepsilon(\omega,z)\exp\left(-\frac{ikz}{\varepsilon^2}\right)\exp\left(-\frac{\varepsilon\beta k^2}{2}m\left(\frac{z}{\varepsilon^2}\right) - \frac{\varepsilon^2\beta^2k^4}{4}m\left(\frac{z}{\varepsilon^2}\right)^2\right), \tag{4.10}$$

which satisfy the linear equation

$$\frac{\partial}{\partial z}\begin{pmatrix} a^\varepsilon \\ b^\varepsilon\end{pmatrix}(\omega,z) = Q^\varepsilon(\omega,z)\begin{pmatrix} a^\varepsilon \\ b^\varepsilon\end{pmatrix}(\omega,z). \tag{4.11}$$

The complex 2×2 matrix Q^ε is given by

$$Q^\varepsilon(\omega,z) = \begin{pmatrix} Q_1^\varepsilon(\omega,z) & Q_2^\varepsilon(\omega,z)e^{\frac{2ikz}{\varepsilon^2}} \\ \overline{Q_2^\varepsilon}(\omega,z)e^{-\frac{2ikz}{\varepsilon^2}} & \overline{Q_1^\varepsilon}(\omega,z)\end{pmatrix} \tag{4.12}$$

FIG. 4.1. *Scattering problem.*

with

$$Q_1^\varepsilon(\omega, z) = -\frac{ik}{2\varepsilon}\left(1+\beta k^2\right) m\left(\frac{z}{\varepsilon^2}\right) - \frac{i\beta^2 k^5}{2} m^2\left(\frac{z}{\varepsilon^2}\right) + O(\varepsilon), \tag{4.13}$$

$$Q_2^\varepsilon(\omega, z) = -\frac{ik}{2\varepsilon}\left(1-\beta k^2\right) m\left(\frac{z}{\varepsilon^2}\right) + \frac{\beta k^2}{2\varepsilon} m'\left(\frac{z}{\varepsilon^2}\right) + \frac{i\beta^2 k^5}{2} m^2\left(\frac{z}{\varepsilon^2}\right)$$

$$+ \frac{\beta^2 k^4}{2} m\left(\frac{z}{\varepsilon^2}\right) m'\left(\frac{z}{\varepsilon^2}\right) + O(\varepsilon). \tag{4.14}$$

The small terms of order ε come from the $O(\varepsilon^3)$ term in the expansion (4.8).

4.2. Boundary values. We assume that a left-going pulse is incoming from the right and is scattered into a reflected wave at $z = 0$ and a transmitted wave at $z = -L/\varepsilon^2$ (see Figure 4.1).

The incoming pulse shape is given by the elevation function $f(t)$, where f is assumed to be a L^1 function compactly supported in the Fourier domain:

$$u_{inc}(t, z=0) = -\int \frac{\omega}{k(\omega)} \hat{f}(\omega) \exp(i\omega t) d\omega, \tag{4.15}$$

$$\eta_{inc}(t, z=0) = \int \hat{f}(\omega) \exp(i\omega t) d\omega, \tag{4.16}$$

with $\mathrm{supp}(\hat{f}) \subset (-1/\sqrt{\beta}, 1/\sqrt{\beta})$. We also impose a radiation condition at $-L/\varepsilon^2$ corresponding to the absence of right-going waves at the left-hand side of the slab $[-L/\varepsilon^2, 0]$. The two-point boundary value problem consisting of the system (4.11) for $z \in [0, L]$, together with the conditions

$$b^\varepsilon(\omega, z=0) = \hat{f}(\omega), \qquad a^\varepsilon(\omega, z=-L) = 0,$$

is then well posed.

4.3. Propagator. It is convenient to transform the two-point boundary value problem into an initial value problem by introducing the propagator $Y^\varepsilon(\omega, -L, z)$, which is a complex 2×2 matrix solution of

$$\frac{\partial Y^\varepsilon}{\partial z}(\omega, -L, z) = Q^\varepsilon(\omega, z) Y^\varepsilon(\omega, -L, z), \qquad Y^\varepsilon(\omega, -L, z=-L) = Id_{\mathbb{C}^2}$$

such that

$$Y^\varepsilon(\omega, -L, z) \begin{pmatrix} a^\varepsilon(\omega, -L) \\ b^\varepsilon(\omega, -L) \end{pmatrix} = \begin{pmatrix} a^\varepsilon(\omega, z) \\ b^\varepsilon(\omega, z) \end{pmatrix}.$$

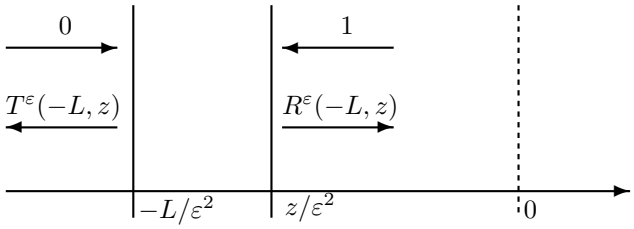

FIG. 4.2. *Reflection and transmission coefficients.*

By the form (4.12) of the matrix Q^ε, if the column vector $(a_1^\varepsilon, b_1^\varepsilon)^T$ is solution of (4.11) with the initial conditions

$$a_1^\varepsilon(\omega,-L)=1, \quad b_1^\varepsilon(\omega,-L)=0, \tag{4.17}$$

then the column vector $(\overline{b_1^\varepsilon}, \overline{a_1^\varepsilon})^T$ is another solution linearly independent of the first solution, so that the propagator matrix Y^ε can be written as

$$Y^\varepsilon(\omega,-L,z)=\begin{pmatrix} a_1^\varepsilon & \overline{b_1^\varepsilon} \\ b_1^\varepsilon & \overline{a_1^\varepsilon} \end{pmatrix}(\omega,z).$$

Note also that the matrix Q^ε has zero trace because $\overline{Q_1^\varepsilon} = -Q_1^\varepsilon$. As a consequence, the determinant of Y^ε is conserved, and $(a_1^\varepsilon, b_1^\varepsilon)$ satisfies the relation

$$\det Y^\varepsilon = |a_1^\varepsilon|^2 - |b_1^\varepsilon|^2 = 1. \tag{4.18}$$

We can now define the *transmission and reflection coefficients* $T^\varepsilon(\omega,-L,z)$ and $R^\varepsilon(\omega,-L,z)$, respectively, for a slab $[-L,z]$ by (see also Figure 4.2)

$$Y^\varepsilon(\omega,-L,z)\begin{pmatrix} 0 \\ T^\varepsilon(\omega,-L,z) \end{pmatrix} = \begin{pmatrix} R^\varepsilon(\omega,-L,z) \\ 1 \end{pmatrix}.$$

In terms of the propagator entries, they are given by

$$R^\varepsilon(\omega,-L,z)=\frac{\overline{b_1^\varepsilon}}{\overline{a_1^\varepsilon}}(\omega,z), \quad T^\varepsilon(\omega,-L,z)=\frac{1}{\overline{a_1^\varepsilon}}(\omega,z),$$

and they satisfy the closed form nonlinear differential system

$$\frac{\partial R^\varepsilon}{\partial z} = 2Q_1^\varepsilon(\omega,z)R^\varepsilon - e^{-\frac{2ikz}{\varepsilon^2}}\overline{Q_2^\varepsilon}(\omega,z)(R^\varepsilon)^2 + e^{\frac{2ikz}{\varepsilon^2}}Q_2^\varepsilon(\omega,z), \tag{4.19}$$

$$\frac{\partial T^\varepsilon}{\partial z} = -T^\varepsilon\left(e^{-\frac{2ikz}{\varepsilon^2}}\overline{Q_2^\varepsilon}(\omega,z)R^\varepsilon + \overline{Q_1^\varepsilon}(\omega,z)\right), \tag{4.20}$$

with the initial conditions at $z=-L$

$$R^\varepsilon(\omega,-L,z=-L)=0, \quad T^\varepsilon(\omega,-L,z=-L)=1.$$

Note that (4.18) implies the conservation of energy relation

$$|R^\varepsilon|^2 + |T^\varepsilon|^2 = 1 \tag{4.21}$$

and in turn the uniform boundedness of the transmission and reflection coefficients. Note also that R^ε and T^ε are the reflection and transmission coefficients for the modified characteristics (4.9)–(4.10). In terms of the real characteristics, the reflection and transmission coefficients are R^ε and $T^\varepsilon \exp(-ikL/\varepsilon^2)$, respectively.

4.4. Quantities of interest. The transmitted wave at time t, denoted by $(u^\varepsilon_{tr}, \eta^\varepsilon_{tr})$, is the left-going wave, which admits the following integral representation in terms of the transmission coefficients:

$$u^\varepsilon_{tr}\left(t, z=-\frac{L}{\varepsilon^2}\right) = -\int \frac{\omega}{k(\omega)}\hat{f}(\omega)T^\varepsilon(\omega,-L,0)\exp\left(i\omega t - ik(\omega)\frac{L}{\varepsilon^2}\right)d\omega, \tag{4.22}$$

$$\eta^\varepsilon_{tr}\left(t, z=-\frac{L}{\varepsilon^2}\right) = \int \hat{f}(\omega)T^\varepsilon(\omega,-L,0)\exp\left(i\omega t - ik(\omega)\frac{L}{\varepsilon^2}\right)d\omega. \tag{4.23}$$

Similarly, the reflected wave $(u^\varepsilon_{ref}, \eta^\varepsilon_{ref})$ can be expressed in terms of the reflection coefficients as

$$u^\varepsilon_{ref}(t, z=0) = \int \frac{\omega}{k(\omega)}\hat{f}(\omega)R^\varepsilon(\omega,-L,0)\exp\left(i\omega t\right)d\omega, \tag{4.24}$$

$$\eta^\varepsilon_{ref}(t, z=0) = \int \hat{f}(\omega)R^\varepsilon(\omega,-L,0)\exp\left(i\omega t\right)d\omega. \tag{4.25}$$

These are the quantities that we will use as new initial conditions for the time reversal experiments.

5. Time reversal setups.

5.1. Time reversal in reflection (TRR). The first step of the time reversal procedure consists of recording the reflected signal at $z = 0$ up to a certain time. It turns out that as $\varepsilon \to 0$ the interesting asymptotic regime arises when we record the signal up to a large time of order $1/\varepsilon^2$, which we denote by t_1/ε^2 with $t_1 > 0$. In the context of shallow water waves, one records only the elevation η_{ref}. If the recording were sufficiently long, one could deduce the depth-averaged velocity u_{ref} by using (4.24), (4.25), but this is not usually the case. If the recording is done over an approximately flat region, then, through (4.15), (4.16) and the proper zero-padding for Fourier transforming the elevation data $\eta_{ref} \equiv f$, the consistent incoming velocity field for the time reversal experiment can be well approximated. The zero-padding is due to the cut-off function of the recorded signal, as explained below.

In the second step of the time reversal procedure a piece of the recorded signal is cut using a cut-off function $s \mapsto G_{t_1}(\varepsilon^2 s)$, where the support of G_{t_1} is included in $[0, t_1]$:

$$\eta^\varepsilon_{ref,cut}\left(\frac{t}{\varepsilon^2}\right) = \eta^\varepsilon_{ref}\left(\frac{t}{\varepsilon^2}\right)G_{t_1}(t).$$

One then time reverses that piece of signal and re-emits the corresponding elevation field with a two-fold amplification. No velocity field is generated. This gives rise to a new wave that can be decomposed as the sum of a right-going wave and a left-going wave. The right-going wave propagates freely in the homogeneous right half-space, and it can be forgotten. The left-going wave is the new incoming signal. Accordingly, the elevation of the time reversed wave sent back into the medium is given by

$$\begin{aligned}\eta^\varepsilon_{inc(TRR)}\left(\frac{t}{\varepsilon^2}, z=0\right) &= \eta^\varepsilon_{ref}\left(\frac{t_1-t}{\varepsilon^2}\right)G_{t_1}(t_1-t)\\ &= \frac{1}{\varepsilon^2}\int\int \exp\left(\frac{i\omega(t_1-t)}{\varepsilon^2}\right)\hat{\eta}^\varepsilon_{ref}(\omega')\hat{G}_{t_1}\left(\frac{\omega-\omega'}{\varepsilon^2}\right)d\omega' d\omega\\ &= \frac{1}{\varepsilon^2}\int\int \exp\left(\frac{i\omega(t-t_1)}{\varepsilon^2}\right)\overline{\hat{\eta}^\varepsilon_{ref}}(\omega')\overline{\hat{G}}_{t_1}\left(\frac{\omega-\omega'}{\varepsilon^2}\right)d\omega' d\omega,\end{aligned} \tag{5.1}$$

where *TRR* stands for "time reversal in reflection." Here we have used the fact that η^ε_{ref} is a real-valued signal, and also that $k(-\omega) = -k(\omega)$, by (4.3), which is actually a direct consequence of the *time reversibility* of the Boussinesq equation. The new incoming (left-going) velocity is given by

$$u^\varepsilon_{inc(TRR)}\left(\frac{t}{\varepsilon^2}, z=0\right) = -\frac{1}{\varepsilon^2}\int\int \frac{\omega}{k(\omega)} e^{\frac{i\omega(t-t_1)}{\varepsilon^2}} \overline{\hat\eta^\varepsilon_{ref}}(\omega')\overline{\hat G}_{t_1}\left(\frac{\omega-\omega'}{\varepsilon^2}\right) d\omega' d\omega. \tag{5.2}$$

A right-going velocity wave is also generated, but it propagates freely with the right-going elevation wave mentioned above, and it can be forgotten as well. Note that the reason why we have amplified the generated elevation field by a factor two is that it gives rise to two counter-propagating waves which both contain half of the generated energy.

The new incoming signal (5.1)–(5.2) repropagates into the same medium and generates a new reflected signal which we observe at the time $t_2/\varepsilon^2 + t$, that is, around the time t_2/ε^2 in the scale of the initial pulse $f(t)$. In terms of the reflection coefficients the observed reflected elevation signal is given by

$$\eta^\varepsilon_{ref(TRR)}\left(\frac{t_2}{\varepsilon^2}+t, z=0\right) = \int \hat\eta^\varepsilon_{inc(TR)}(\omega) R^\varepsilon(\omega, -L, 0) e^{\frac{i\omega t_2}{\varepsilon^2}+i\omega t} d\omega.$$

Substituting the expression of $\hat\eta^\varepsilon_{inc(TRR)}$ into this equation yields the following representation of the reflected signal:

$$\eta^\varepsilon_{ref(TRR)}\left(\frac{t_2}{\varepsilon^2}+t, z=0\right) = \frac{1}{\varepsilon^2}\int\int e^{i\omega t} e^{\frac{i\omega(t_2-t_1)}{\varepsilon^2}} \overline{\hat f}(\omega')\overline{\hat G}_{t_1}\left(\frac{\omega-\omega'}{\varepsilon^2}\right) \times R^\varepsilon(\omega, -L, 0)\overline{R^\varepsilon}(\omega', -L, 0) d\omega' d\omega.$$

After the change of variable $\omega' = \omega - \varepsilon^2 h$, the representation becomes

$$\eta^\varepsilon_{ref(TRR)}\left(\frac{t_2}{\varepsilon^2}+t, z=0\right) = \int\int e^{i\omega t} e^{\frac{i\omega(t_2-t_1)}{\varepsilon^2}} \overline{\hat f}(\omega-\varepsilon^2 h)\overline{\hat G}_{t_1}(h) \times R^\varepsilon(\omega, -L, 0)\overline{R^\varepsilon}(\omega-\varepsilon^2 h, -L, 0) dh\, d\omega. \tag{5.3}$$

Note that, by (4.21), the reflection coefficients are bounded, and we shall show in section 6 that the rapid phase $\exp(i\omega(t_2-t_1)/\varepsilon^2)$ averages out the integral except when $t_2 = t_1$. This means that refocusing can be observed only at the time $t_2/\varepsilon^2 = t_1/\varepsilon^2$. The precise description of the refocused pulse, taking into account the interaction between randomness and dispersion, will be carried out in section 6.

5.2. Transmitted front wave. Before going into time reversal in transmission, we give an integral representation for the *coherent transmitted wavefront* observed at $z = -L/\varepsilon^2$ around the effective arrival time L/ε^2. By (4.23), the transmitted elevation front is given by

$$\eta^\varepsilon_{tr}\left(\frac{L}{\varepsilon^2}+t, z=-\frac{L}{\varepsilon^2}\right) = \int e^{i\omega t} e^{i(\omega-k(\omega))\frac{L}{\varepsilon^2}} \hat f(\omega) T^\varepsilon(\omega, -L, 0) d\omega. \tag{5.4}$$

Note that expressions like $t + L$ arise because constants have been set to one, so that the mean velocity is one. Due to dispersion, $k(\omega)$ is different from ω (see (4.3)). As a consequence, if $\beta = O(1)$, then the rapid phase $\exp(i(\omega - k(\omega))L/\varepsilon^2)$ makes the integral vanish as $\varepsilon \to 0$. This is in dramatic contrast with the hyperbolic case ($\beta = 0$),

where the coherent transmitted wave persists in this regime as a manifestation of the well known O'Doherty–Anstey theory studied in [8, 17, 25] in various situations.

In the dispersive case, the front will be present if the dispersion parameter β is small enough. This has been characterized and observed numerically in [18]. In particular, in the regime where $\beta = \varepsilon^2\beta_0$, we can derive the precise shape of the front resulting from the interplay of randomness and dispersion. In that regime, by expanding the dispersion relation $\omega \mapsto k(\omega)$, we get that the front is given by

$$\eta^\varepsilon_{tr}\left(\frac{L}{\varepsilon^2}+t, z=-\frac{L}{\varepsilon^2}\right) = \int e^{i\omega t}e^{-i\beta_0\omega^3 L}\hat{f}(\omega)T^\varepsilon(\omega,-L,0)d\omega + O(\varepsilon^2).$$

The transmission coefficients are given by $T^\varepsilon(\omega,-L,0) = 1/\overline{a^\varepsilon_1}(\omega,0)$, where a^ε_1 satisfies (4.11) with the initial conditions (4.17). In the case $\beta = \varepsilon^2\beta_0$, the entries of the matrix Q^ε can be expanded as

$$Q^\varepsilon_1(\omega,z)|_{\beta=\beta_0\varepsilon^2} = -\frac{ik}{2\varepsilon}m\left(\frac{z}{\varepsilon^2}\right) + O(\varepsilon),$$
$$Q^\varepsilon_2(\omega,z)|_{\beta=\beta_0\varepsilon^2} = -\frac{ik}{2\varepsilon}m\left(\frac{z}{\varepsilon^2}\right) + O(\varepsilon),$$

so that we get the same system as in the hyperbolic case up to terms of order ε. The limit of η^ε_{tr} has been derived for the hyperbolic case with small fluctuations [2, 25]. In our case the derivation of the limit follows the same lines except for the deterministic phase $\exp(-i\beta_0\omega^3 L)$ due to the small dispersion. The process $(\eta^\varepsilon_{tr}(\frac{L}{\varepsilon^2}+t, z=-\frac{L}{\varepsilon^2}))_{t\in(-\infty,+\infty)}$ converges in the space of the continuous and bounded functions to

$$\eta_{tr}(t) = \int \hat{f}(\omega)\exp\left(i\omega\left(t-\frac{\sqrt{\gamma(0)}}{\sqrt{2}}B_L\right) - \frac{\omega^2\gamma(\omega)}{4}L - i\beta_0\omega^3 L\right)d\omega,$$

where B_L is a standard Brownian motion and γ is

$$\gamma(\omega) = \int_0^\infty \mathbb{E}[m(0)m(z)]e^{2i\omega z}dz. \tag{5.5}$$

Using convolution operators, the transmitted front can be written in a simpler form

$$\eta_{tr}(t) = f * K\left(t-\frac{\sqrt{\gamma(0)}}{\sqrt{2}}B_L\right), \tag{5.6}$$

which means that a random Gaussian centering appears through the Brownian motion B_L, while the pulse shape spreads in a deterministic way through the convolution by the kernel K,

$$K(t) = K_r * K_d(t).$$

Here K_d is the scaled Airy function [1]

$$K_d(t) = \frac{1}{(3\beta_0 L)^{1/3}}\mathrm{Ai}\left(-\frac{t}{(3\beta_0 L)^{1/3}}\right),$$

and the Fourier transform of K_r is

$$\hat{K}_r(\omega) = \exp\left(-\frac{\omega^2\gamma(\omega)L}{4}\right).$$

Note that the kernel K depends both on randomness (through the function γ) and on dispersion (through the parameter β_0). This stochastic formulation is in agreement with the formulation presented in [18] for small β and was validated numerically with the same code used in this paper.

Observe that a dispersion parameter $\beta = O(1)$ or even $O(\varepsilon^p)$ with $p < 2$ leaves a fast phase in the integral representation of the transmitted front, as can be seen in (5.4). This implies a dramatic spreading of the pulse for a propagation distance of order $1/\varepsilon^2$, so that no coherent front pulse can be observed at the output $z = -L/\varepsilon^2$. In that case we are led to perform time reversal using the coda of the transmitted wave containing the incoherent fluctuations.

5.3. Time reversal in transmission (TRT). We now come back to the case of a dispersion parameter β of order 1. The time reversal procedure consists of recording the transmitted coda signal at $z = -L/\varepsilon^2$ over the time interval $[(L + t_0)/\varepsilon^2, (L + t_1)/\varepsilon^2]$. A piece of the recorded signal is cut using a cut-off function $s \mapsto G_{t_0,t_1}(\varepsilon^2 s - L)$, where the support of G_{t_0,t_1} is included in $[t_0, t_1]$:

$$\eta^\varepsilon_{tr,cut}\left(\frac{t}{\varepsilon^2}\right) = \eta^\varepsilon_{tr}\left(\frac{L+t}{\varepsilon^2}, z = -\frac{L}{\varepsilon^2}\right) G_{t_0,t_1}(t).$$

One then time reverses that piece of signal and sends it back into the same medium. As in section 5.1 one usually (only) records the elevation η_{tr}. Since the velocity field is not recorded, one actually generates the time reversed elevation field with an amplification by two, which in turn generates two counter-propagating waves with equal energies. Numerically we can record both the wave elevation and the velocity field. We will present examples comparing these two cases and show that the refocused pulse is the same. The elevation of the wave sent back is given by

$$\begin{aligned}\eta^\varepsilon_{inc(TRT)}\left(\frac{t}{\varepsilon^2}, z = -\frac{L}{\varepsilon^2}\right) &= \eta^\varepsilon_{tr}\left(\frac{L+t_1-t}{\varepsilon^2}, z = -\frac{L}{\varepsilon^2}\right) G_{t_0,t_1}(t_1 - t)\\ &= \frac{1}{\varepsilon^2}\int\int \exp\left(\frac{i\omega(t_1-t)}{\varepsilon^2}\right)\hat\eta^\varepsilon_{tr}(\omega')\hat G_{t_0,t_1}\left(\frac{\omega-\omega'}{\varepsilon^2}\right)d\omega' d\omega,\end{aligned}$$

where $\hat\eta^\varepsilon_{tr}$ is the Fourier transform of the shifted received signal $t \mapsto \eta^\varepsilon_{tr}(\frac{L+t}{\varepsilon^2}, z = -\frac{L}{\varepsilon^2})$:

$$\hat\eta^\varepsilon_{tr}(\omega) = e^{i(\omega - k(\omega))\frac{L}{\varepsilon^2}}\hat f(\omega) T^\varepsilon(\omega, -L, 0).$$

Also $\eta^\varepsilon_{inc(TRT)}$ reads as

$$\eta^\varepsilon_{inc(TRT)}\left(\frac{t}{\varepsilon^2}, z = -\frac{L}{\varepsilon^2}\right) = \frac{1}{\varepsilon^2}\int\int \exp\left(\frac{i\omega(t-t_1)}{\varepsilon^2}\right)\overline{\hat\eta^\varepsilon_{tr}}(\omega')\overline{\hat G}_{t_0,t_1}\left(\frac{\omega-\omega'}{\varepsilon^2}\right)d\omega' d\omega.$$

Let us denote by $\tilde R^\varepsilon$ and $\tilde T^\varepsilon$ the reflection and transmission coefficients for the experiment corresponding to a right-going input wave incoming from the left (see Figure 5.1). Using the propagator Y^ε defined in section 4.3, $\tilde R^\varepsilon$ and $\tilde T^\varepsilon$ obey the relation

$$Y^\varepsilon(\omega, -L, 0)\begin{pmatrix} 1 \\ \tilde R^\varepsilon(\omega, -L, 0)\end{pmatrix} = \begin{pmatrix} \tilde T^\varepsilon(\omega, -L, 0) \\ 0\end{pmatrix}.$$

In terms of the propagator entries they are given by

$$\tilde R^\varepsilon(\omega, -L, 0) = -\frac{b^\varepsilon_1}{a^\varepsilon_1}(\omega, 0), \qquad \tilde T^\varepsilon(\omega, -L, 0) = \frac{1}{a^\varepsilon_1}(\omega, 0),$$

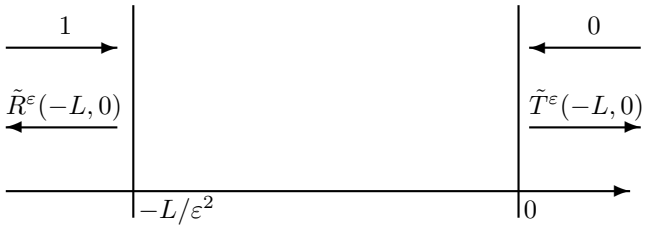

FIG. 5.1. *Adjoint reflection and transmission coefficients for time reversal.*

which shows that

$$\tilde{T}^\varepsilon(\omega,-L,0)=T^\varepsilon(\omega,-L,0).$$

Accordingly, the new incoming signal repropagates into the same medium and generates a new transmitted signal, which we observe at the time t_2/ε^2+t, that is, around the time t_2/ε^2 in the scale of the initial pulse $f(t)$. In terms of the transmission coefficients, the observed transmitted elevation signal is given by

$$\eta^\varepsilon_{tr(TRT)}\left(\frac{t_2}{\varepsilon^2}+t,z=0\right)=\int\hat{\eta}^\varepsilon_{inc(TRT)}(\omega)T^\varepsilon(\omega,-L,0)e^{\frac{i\omega t_2}{\varepsilon^2}+i\omega t}e^{-ik(\omega)\frac{L}{\varepsilon^2}}d\omega.$$

Substituting the expression of $\hat{\eta}^\varepsilon_{inc(TRT)}$ into this equation yields the following representation of the new transmitted signal:

$$\eta^\varepsilon_{tr(TRT)}\left(\frac{t_2}{\varepsilon^2}+t,z=0\right)=\frac{1}{\varepsilon^2}\int\int e^{i\omega t}e^{\frac{i\omega(t_2-t_1-L)}{\varepsilon^2}}\overline{\hat{f}}(\omega')\overline{\hat{G}}_{t_0,t_1}\left(\frac{\omega-\omega'}{\varepsilon^2}\right)$$
$$\times e^{i(k(\omega')-k(\omega))\frac{L}{\varepsilon^2}}e^{-i(\omega'-\omega)\frac{L}{\varepsilon^2}}T^\varepsilon(\omega,-L,0)\overline{T^\varepsilon}(\omega',-L,0)d\omega'd\omega.$$

After the change of variable $\omega'=\omega-\varepsilon^2h$, the representation becomes

$$\eta^\varepsilon_{tr(TRT)}\left(\frac{t_2}{\varepsilon^2}+t,z=0\right)=\int\int e^{i\omega t}e^{\frac{i\omega(t_2-t_1-L)}{\varepsilon^2}}\overline{\hat{f}}(\omega-\varepsilon^2h)\overline{\hat{G}}_{t_0,t_1}(h)$$
$$\times e^{i(k(\omega-\varepsilon^2h)-k(\omega))\frac{L}{\varepsilon^2}}e^{ihL}T^\varepsilon(\omega,-L,0)\overline{T^\varepsilon}(\omega-\varepsilon^2h,-L,0)dh\;d\omega. \tag{5.7}$$

The precise asymptotics of the transmitted wave will be carried out in section 7. It is easily seen that the refocusing will only take place if $t_2=L+t_1$ due to the fast phase.

5.4. TRT in homogeneous medium. One application of TRT is source reconstruction when the medium is known. This is motivated by the problem of waveform inversion for water waves studied in [24], where the goal is to characterize the initial sea surface displacement due to tsunamigenic earthquakes. Mathematically, in the context of this paper, the source inversion problem consists of performing TRT. The repropagation of the time reversed transmitted wave is performed by solving numerically the corresponding wave equation. In the case of the time reversal experiment for a dispersive homogeneous medium, we observe a transmitted signal and would like to recover both the location and the pulse shape of the source. This implies the recompression of the dispersive oscillatory coda of the transmitted wave. Dispersion helps with the source location identification. This is in contrast with (traveling) hyperbolic waves in a homogeneous medium.

Taking $T^\varepsilon = 1$ in (5.7) gives the transmitted signal in homogeneous medium. Observe that the quantities become independent of ε, so that ε can be taken to be equal to 1. We then get

$$\eta_{tr(TRT)}(t_1+L+t,z) = \int\int e^{i\omega t - ik(\omega)z}\overline{\hat{f}}(\omega-h)\overline{\hat{G}}_{t_0,t_1}(h)e^{i(k(\omega-h)-k(\omega))L}e^{ihL}dh\ d\omega,$$

where we look at two cases, as follows.

(a) Hyperbolic case. If $\beta = 0$, then $k(\omega) = \omega$, and so the transmitted wave is

$$\eta_{tr(TRT)}(t_1+L+t,z) = \int\int e^{i\omega(t-z)}\overline{\hat{f}}(\omega-h)\overline{\hat{G}}_{t_0,t_1}(h)dh\ d\omega,$$

which yields a traveling wave

$$\eta_{tr(TRT)}(t_1+L+t,z) = (G_{t_0,t_1}f)(z-t).$$

On the one hand, it is impossible to retrieve the source location from this traveling wave. On the other hand, as soon as the support of the cut-off function is larger than the pulse width, then the reconstruction of the pulse shape is perfect.

(b) Dispersive case. If $\beta \neq 0$ and $(\beta L)^{1/3}$ is much larger than the pulse width, then

$$\eta_{tr(TRT)}(t_1+L+t,z) = K_{z,L} * f(z-t),$$

where the kernel $K_{z,L}$ is given by

$$\begin{aligned} K_{z,L}(t) &= K_z * K_L(t), \\ K_z(t) &= \frac{1}{(3\beta z)^{1/3}}\mathrm{Ai}\left(\frac{t}{(3\beta z)^{1/3}}\right), \\ \hat{K}_L(\omega) &= G_{t_0,t_1}\left(((1+\beta k(\omega)^2)^{3/2}-1)L\right). \end{aligned}$$

The Airy kernel K_z results from the action of dispersion on the refocused pulse around the original source location. Let us define $z_c = T_w^3/(3\beta)$, where T_w is the pulse width. If $z < -z_c$, then pulse refocusing is not yet completed and the oscillatory tail is not yet recompressed. If $z > z_c$, then the pulse starts developing the dispersive tail again. When $z \in [-z_c, z_c]$, the oscillatory tail vanishes and the kernel $K_z$is close to a Dirac mass. This shows that *dispersion enhances the resolution of the source location* since z_c decays with increasing β. However *the reconstruction of the source shape is blurred by dispersive effects* since the cut-off function G deletes a frequency band that becomes larger as β is larger.

6. Asymptotics of the refocused pulse in reflection. From now on we assume that β is of order 1. The integral representation (5.3) of the reflected signal shows that the autocorrelation function of the reflection coefficient at two nearby frequencies will play an important role.

6.1. The frequency autocorrelation function of the reflection coefficient. We shall study the symmetric version

$$U^\varepsilon_{1,1}(\omega,h,z) = R^\varepsilon\left(\omega+\frac{\varepsilon^2 h}{2},-L,z\right)\overline{R^\varepsilon}\left(\omega-\frac{\varepsilon^2 h}{2},-L,z\right),$$

and we shall extend the approach developed in [2, 7] to the dispersive case. It is necessary to consider a family of moments so as to get a closed system of equations. We thus introduce for $n, p \in \mathbb{N}$

$$U^{\varepsilon}_{n,p}(\omega, h, z) = \left(R^{\varepsilon}\left(\omega + \frac{\varepsilon^2 h}{2}, -L, z\right)\right)^n \left(\overline{R^{\varepsilon}}\left(\omega - \frac{\varepsilon^2 h}{2}, -L, z\right)\right)^p.$$

Denoting

$$k'(\omega) = \frac{\partial k}{\partial \omega}(\omega) = \frac{1}{(1-\beta\omega^2)^{3/2}} = (1+\beta k^2)^{3/2} \tag{6.1}$$

and using the Riccati equation (4.19) satisfied by R^{ε}, we deduce

$$\begin{aligned}\frac{\partial U^{\varepsilon}_{n,p}}{\partial z} &= 2(n-p)Q^{\varepsilon}_1 U^{\varepsilon}_{n,p} + Q^{\varepsilon}_2 e^{\frac{2ik(\omega)z}{\varepsilon^2}}\left(ne^{ik'(\omega)hz}U^{\varepsilon}_{n-1,p} - pe^{-ik'(\omega)hz}U^{\varepsilon}_{n,p+1}\right)\\ &\quad + \overline{Q^{\varepsilon}_2} e^{-\frac{2ik(\omega)z}{\varepsilon^2}}\left(pe^{ik'(\omega)hz}U^{\varepsilon}_{n,p-1} - ne^{-ik'(\omega)hz}U^{\varepsilon}_{n+1,p}\right)\end{aligned}$$

starting from

$$U^{\varepsilon}_{n,p}(\omega, h, z = -L) = \mathbf{1}_0(n)\mathbf{1}_0(p),$$

where $\mathbf{1}_0(n) = 1$ if $n = 0$ and 0 otherwise. Taking a shifted scaled Fourier transform with respect to h,

$$V^{\varepsilon}_{n,p}(\omega, \tau, z) = \frac{k'(\omega)}{2\pi}\int e^{ihk'(\omega)(\tau-(n+p)z)}U^{\varepsilon}_{n,p}(\omega, h, z)dh,$$

we get

$$\begin{aligned}\frac{\partial V^{\varepsilon}_{n,p}}{\partial z} &= -(n+p)\frac{\partial V^{\varepsilon}_{n,p}}{\partial \tau} + 2(n-p)Q^{\varepsilon}_1 V^{\varepsilon}_{n,p}\\ &\quad + Q^{\varepsilon}_2 e^{\frac{2ik(\omega)z}{\varepsilon^2}}\left(nV^{\varepsilon}_{n-1,p} - pV^{\varepsilon}_{n,p+1}\right) + \overline{Q^{\varepsilon}_2} e^{-\frac{2ik(\omega)z}{\varepsilon^2}}\left(pV^{\varepsilon}_{n,p-1} - nV^{\varepsilon}_{n+1,p}\right)\end{aligned}$$

starting from

$$V^{\varepsilon}_{n,p}(\omega, \tau, z = -L) = \delta(\tau)\mathbf{1}_0(n)\mathbf{1}_0(p).$$

Applying a diffusion-approximation theorem [2, section 3] establishes that the processes $V^{\varepsilon}_{n,p}$ converge to diffusion processes as $\varepsilon \to 0$. In particular, the expectations $\mathbb{E}[V^{\varepsilon}_{n,n}(\omega, \tau, z)]$, $n \in \mathbb{N}$, converge to $W_n(\omega, \tau, z)$, which obey the closed system of transport equations

$$\begin{aligned}&\frac{\partial W_n}{\partial z} + 2n\frac{\partial W_n}{\partial \tau} = \frac{1}{2}\alpha_\beta(\omega)k(\omega)^2 n^2\left(W_{n+1} + W_{n-1} - 2W_n\right),\\ &W_n(\omega, \tau, z = -L) = \delta(\tau)\mathbf{1}_0(n),\end{aligned} \tag{6.2}$$

where

$$\alpha_\beta(\omega) = \alpha(k(\omega))(1+\beta k(\omega)^2)^2 = \frac{\alpha(\omega/\sqrt{1-\beta\omega^2})}{(1-\beta\omega^2)^2} \tag{6.3}$$

and α is proportional to the power spectral density of the random process m:

$$\alpha(k) = \int_0^\infty \mathbb{E}[m(0)m(z)]\cos(2kz)dz. \tag{6.4}$$

Note that the limit transport equations (6.2) have the same form as those obtained in the nondispersive case in [2]. The difference is contained in the rate coefficient $\alpha_\beta(\omega)k(\omega)^2$, which is simply $\alpha_0(\omega)\omega^2$ in the hyperbolic case. We then get the limit of the autocorrelation function of the reflection coefficient:

$$\mathbb{E}\left[R^\varepsilon\left(\omega+\frac{\varepsilon^2 h}{2},-L,0\right)\overline{R^\varepsilon}\left(\omega-\frac{\varepsilon^2 h}{2},-L,0\right)\right]\overset{\varepsilon\to 0}{\longrightarrow}\int\Lambda^L_{ref}(\omega,\tau)e^{-ih\tau}d\tau, \tag{6.5}$$

$$\Lambda^L_{ref}(\omega,\tau)=k'(\omega)^{-1}W_1(\omega,k'(\omega)^{-1}\tau,0). \tag{6.6}$$

The quantity $W_1(\omega,\tau,0)$ is obtained through the system of transport equations (6.2), which we study in the next section.

6.2. Analysis of the transport equations. We can interpret the transport equation (6.2) in terms of a jump Markov process. Let us introduce the process $(N_t)_{t\geq 0}$ with state space $\mathbb{N}$ and infinitesimal generator

$$\mathcal{L}\phi(N)=\frac{1}{2}\alpha_\beta(\omega)k(\omega)^2N^2\left(\phi(N+1)+\phi(N-1)-2\phi(N)\right).$$

As in [2], we deduce

$$\int_{\tau_0}^{\tau_1}W_1(\omega,\tau,0)d\tau=\mathbb{P}_1\left(\int_0^L 2N_s ds\in[\tau_0,\tau_1],\ N_L=0\right),$$

where $\mathbb{P}_{p_0}$ stands for the probability over the distribution of the jump process starting from $N_0=p_0$. Taking $\tau_0=0$ and $\tau_1=\infty$ yields

$$\mathbb{E}\left[|R^\varepsilon|^2(\omega,-L,0)\right]\overset{\varepsilon\to 0}{\longrightarrow}\mathbb{P}_1(N_L=0).$$

It is remarkable that the generating function of the jump process can be expressed in terms of the expectation of some functional of the diffusion process $(\theta_t)_{t\geq 0}$:

$$d\theta_t=\sqrt{\alpha_\beta(\omega)}k(\omega)dB_t+\frac{1}{2}\alpha_\beta(\omega)k(\omega)^2\coth(\theta_t)dt. \tag{6.7}$$

We have

$$\mathbb{E}_{p_0}\left[z^{N_t}\right]=\mathbb{E}\left[\tanh\left(\frac{\theta_t}{2}\right)^{2p_0}\ \middle|\ \theta_0=2\ \mathrm{argtanh}(\sqrt{z})\right],$$

where $\mathbb{E}_{p_0}$ stands for the expectation with respect to the distribution of the jump process starting from $N_0=p_0$. In particular,

$$\mathbb{E}\left[|R^\varepsilon|^2(\omega,-L,0)\right]\overset{\varepsilon\to 0}{\longrightarrow}\mathbb{P}_1(N_L=0)=\mathbb{E}\left[\tanh\left(\frac{\theta_L}{2}\right)^2\ \middle|\ \theta_0=0\right].$$

As the probability density function of the diffusion process (θ_t) is known [21], we get

$$\mathbb{E}\left[|R^\varepsilon|^2(\omega,-L,0)\right]\overset{\varepsilon\to 0}{\longrightarrow}1-\frac{4}{\sqrt{\pi}}\exp\left(-\frac{L}{l_\beta(\omega)}\right)\int_0^\infty\frac{x^2e^{-x^2}}{\cosh\left(2\sqrt{L/l_\beta(\omega)}x\right)}dx,$$

where the localization length $l_\beta(\omega)$ of the mean transmittance is affected by the dispersion

$$l_\beta(\omega) = \frac{8}{\alpha_\beta(k(\omega))k(\omega)^2} = \frac{8(1-\beta\omega^2)^3}{\alpha(\omega/\sqrt{1-\beta\omega^2}))\omega^2}. \tag{6.8}$$

If the power spectral density of the process m can be considered as constant $\alpha(k) \equiv \alpha_0$, that is to say, when the correlation length of the medium is smaller than the typical wavelength of the pulse, then the above expression of the localization length shows that *dispersion enhances localization effects*. The decay of the localization length as a function of frequency is faster in the dispersive case than in the hyperbolic case. This has been observed numerically in [18].

6.3. The refocused pulse. Choosing $t_2 = t_1$ in (5.3) shows that the refocused pulse at $z = 0$ is given by the integral representation

$$\begin{aligned}\eta^\varepsilon_{ref(TRR)}\left(\frac{t_1}{\varepsilon^2}+t, z=0\right) = \int\int e^{i\omega t}\overline{\hat{f}}(\omega-\varepsilon^2 h)\overline{\hat{G}}_{t_1}(h) \\ \times R^\varepsilon(\omega,-L,0)\overline{R^\varepsilon}(\omega-\varepsilon^2 h,-L,0)dh\, d\omega.\end{aligned} \tag{6.9}$$

The main result of this section is the *self-averaging property* of the refocused pulse. This is shown in the following theorem, which gives the convergence of the refocused pulse to a deterministic shape.

THEOREM 6.1. *For any $T > 0$, $\delta > 0$,*

$$\mathbb{P}\left(\sup_{t\in[-T,T]}\left|\eta^\varepsilon_{ref(TRR)}\left(\frac{t_1}{\varepsilon^2}+t, z=0\right) - \eta_{ref(TRR)}(t)\right| > \delta\right) \overset{\varepsilon\to 0}{\longrightarrow} 0,$$

where $\eta_{ref(TRR)}$ is the deterministic pulse shape:

$$\eta_{ref(TRR)}(t) = \left(f(-\,\cdot) * K_{TRR}(\cdot)\right)(t). \tag{6.10}$$

The Fourier transform of the kernel K_{TRR} is the convolution of the time-inverted cut-off function G_{t_1} with the density $\tau \mapsto \Lambda^L_{ref}(\omega,\tau)$ evaluated at 0:

$$\hat{K}_{TRR}(\omega) = \left(G_{t_1}(-\,\cdot) * \Lambda^L_{ref}(\omega,\cdot)\right)(0) = \int G_{t_1}(\tau)\Lambda^L_{ref}(\omega,\tau)d\tau. \tag{6.11}$$

Proof. The first step consists of proving the tightness (i.e., the relative compactness) in the space of continuous trajectories (equipped with the topology associated to the sup norm over the compact subsets) of the family of continuous processes

$$\left(\left(\eta^\varepsilon_{ref(TRR)}\left(\frac{t_1}{\varepsilon^2}+t, z=0\right)\right)_{-\infty<t<\infty}\right)_{\varepsilon>0}.$$

From (6.9) and the uniform bound $|R^\varepsilon| \le 1$, it is easily seen that the quantity $|\eta^\varepsilon_{ref(TRR)}(t_1/\varepsilon^2 + t, z = 0)|$ is uniformly bounded by

$$\int |\hat{G}(h)|dh \times \int |\hat{f}(\omega)|d\omega,$$

which we assume finite. The modulus of continuity

$$\Omega^\varepsilon(s) = \sup_{|s_1-s_2|\le s} \left| \eta^\varepsilon_{ref(TRR)}\left(\frac{t_1}{\varepsilon^2}+s_1, z=0\right) - \eta^\varepsilon_{ref(TRR)}\left(\frac{t_1}{\varepsilon^2}+s_2, z=0\right)\right|$$

is bounded by

$$\Omega^\varepsilon(s) \le \int |\hat{G}(h)|dh \times \int \sup_{|s_1-s_2|\le s} |e^{i\omega(s_2-s_1)}-1||\hat{f}(\omega)|d\omega,$$

which goes to zero as $s \to 0$ uniformly with respect to ε, by Lebesgue's theorem, and ensures tightness.

Taking the expectation in (6.9) and using (6.5), we get the convergence of the first moment:

$$\begin{aligned}\lim_{\varepsilon\to 0} \mathbb{E}\left[\eta^\varepsilon_{ref(TRR)}\left(\frac{t_1}{\varepsilon^2}+t, z=0\right)\right] &= \int\int e^{i\omega t}\overline{\hat{f}}(\omega)\overline{\hat{G}}_{t_1}(h)\int e^{-ih\tau}\Lambda^L_{ref}(\omega,\tau)d\tau dh d\omega \\ &= \int\int e^{i\omega t}\overline{\hat{f}}(\omega)G_{t_1}(\tau)\Lambda^L_{ref}(\omega,\tau)d\tau d\omega \\ &= \left(f(-\,.) * K_{TRR}(.)\right)(t) = \eta_{ref(TRR)}(t).\end{aligned}$$

In order to prove the convergence in probability of $\eta^\varepsilon_{ref(TRR)}(t_1/\varepsilon^2+t, z=0)$ to the deterministic refocused pulse $\eta_{ref(TRR)}$, we compute its second moment and show that it converges to the square of the first moment obtained above. This computation has been done in the acoustic case [9] using the moment analysis of the reflected signal established in [7]. The second moment involves the moment of the product of the reflection coefficients at four frequencies. The presence of the cut-off function G_{t_1} used in time reversal automatically pairs the frequencies. The moment analysis then shows that the reflection coefficients for the two pairs become independent, which proves the result. The same techniques apply to the dispersive case since the Riccati equation (4.19) for the reflection coefficient has the same form as in the acoustic case. □

As for acoustic waves, the case of a large slab (L large) leads to explicit formulas for the refocused pulse. This is developed in the following section.

6.4. Large slab. For acoustic waves the hyperbolicity of the equations makes the reflected quantities of interest independent of L for L large enough. This leads to explicit formulas for the power spectral density Λ^L_{ref}. In our context of dispersive waves, the velocities of the waves are still bounded as we consider a pulse with compactly supported spectrum. For this reason, the power spectral density also becomes independent of L for L large enough. Applying the same approach as in [2] (where the case of acoustic waves was addressed), we get that the function Λ^L_{ref} converges as L grows to infinity to the limit density

$$\Lambda^\infty_{ref}(\omega,\tau) = \frac{\kappa_\beta(\omega)\omega^2}{\left(1+\kappa_\beta(\omega)\omega^2\tau\right)^2}, \tag{6.12}$$

where

$$\kappa_\beta(\omega) = \frac{\alpha_\beta(\omega)k(\omega)^2}{4\omega^2 k'(\omega)} = \frac{\alpha(\omega/\sqrt{1-\beta\omega^2})}{4\left(1-\beta\omega^2\right)^{3/2}}.$$

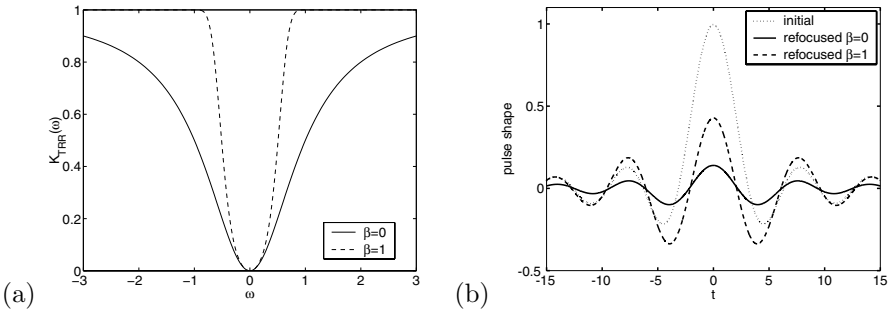

FIG. 6.1. *Fourier transform of the convolution kernel* K_{TRR} (a) *and refocused pulse* (b). *We consider a square cut-off function* $G(t) = \mathbf{1}_{[0,t_1]}(t)$, *and we assume* $\alpha(\omega) \equiv 4$, $t_1 = 1$. *The initial pulse has sinc shape* $f(t) = \sin(t)/t$, *and its spectrum is* $\hat{f}(\omega) = (1/2)\mathbf{1}_{[-1,1]}(\omega)$. *(Note that* $\beta = 1$ *corresponds to a very dispersive configuration.)*

The deterministic refocused pulse is then given by (6.10) with the explicit Λ^{∞}_{ref} derived in this section. Taking, for instance, a square cut-off function $G_{t_1}(t) = \mathbf{1}_{[0,t_1]}(t)$, the kernel K_{TRR} reads as a high-band filter because its Fourier transform is

$$\hat{K}_{TRR}(\omega) = \frac{\kappa_\beta(\omega)\omega^2 t_1}{1 + \kappa_\beta(\omega)\omega^2 t_1}. \tag{6.13}$$

An example is presented in Figure 6.1. The cut-off frequency of the filter $\hat{K}_{TRR}$ decays with increasing dispersion parameter β. This shows that time reversal focusing in reflection is more efficient in the dispersive case than in the hyperbolic case. This is consistent with the observation that localization effects are enhanced in the presence of dispersion (see (6.8)).

7. Asymptotics of refocused pulse in transmission.

7.1. The frequency autocorrelation function of the transmission coefficient. We study here the autocorrelation function of the transmission coefficient at two nearby frequencies. We first define a new family of processes indexed by $n, p \in \mathbb{N}$,

$$\tilde{U}^{\varepsilon}_{n,p}(\omega, h, z) = U^{\varepsilon}_{n,p}(\omega, h, z) T^{\varepsilon}\left(\omega + \frac{\varepsilon^2 h}{2}, -L, z\right) \overline{T^{\varepsilon}}\left(\omega - \frac{\varepsilon^2 h}{2}, -L, z\right),$$

which satisfy

$$\begin{aligned}\frac{\partial \tilde{U}^{\varepsilon}_{n,p}}{\partial z} &= 2(n-p)Q^{\varepsilon}_1 \tilde{U}^{\varepsilon}_{n,p} + Q^{\varepsilon}_2 e^{\frac{2ik(\omega)z}{\varepsilon^2}}\left(n e^{ik'(\omega)hz}\tilde{U}^{\varepsilon}_{n-1,p} - (p+1)e^{-ik'(\omega)hz}\tilde{U}^{\varepsilon}_{n,p+1}\right) \\ &\quad + \overline{Q^{\varepsilon}_2} e^{-\frac{2ik(\omega)z}{\varepsilon^2}}\left(p e^{ik'(\omega)hz}\tilde{U}^{\varepsilon}_{n,p-1} - (n+1)e^{-ik'(\omega)hz}\tilde{U}^{\varepsilon}_{n+1,p}\right)\end{aligned}$$

starting from

$$\tilde{U}^{\varepsilon}_{n,p}(\omega, h, z = -L) = \mathbf{1}_0(n)\mathbf{1}_0(p).$$

Taking a shifted scaled Fourier transform with respect to h,

$$\tilde{V}^{\varepsilon}_{n,p}(\omega, \tau, z) = \frac{k'(\omega)}{2\pi}\int e^{ihk'(\omega)(\tau - (n+p)z)}\tilde{U}^{\varepsilon}_{n,p}(\omega, h, z)dh,$$

we get

$$\frac{\partial \tilde{V}^{\varepsilon}_{n,p}}{\partial z} = -(n+p)\frac{\partial \tilde{V}^{\varepsilon}_{n,p}}{\partial \tau} + 2(n-p)Q^{\varepsilon}_1 \tilde{V}^{\varepsilon}_{n,p}$$
$$+ Q^{\varepsilon}_2 e^{\frac{2ik(\omega)z}{\varepsilon^2}} \left(n\tilde{V}^{\varepsilon}_{n-1,p} - (p+1)\tilde{V}^{\varepsilon}_{n,p+1} \right) + \overline{Q^{\varepsilon}_2} e^{-\frac{2ik(\omega)z}{\varepsilon^2}} \left(p\tilde{V}^{\varepsilon}_{n,p-1} - (n+1)\tilde{V}^{\varepsilon}_{n+1,p} \right)$$

starting from

$$\tilde{V}^{\varepsilon}_{n,p}(\omega, \tau, z = -L) = \delta(\tau)\mathbf{1}_0(n)\mathbf{1}_0(p).$$

Applying a diffusion-approximation theorem [2, section 3.14] establishes that the processes $\tilde{V}^{\varepsilon}_{n,p}$ converge to diffusion processes as $\varepsilon \to 0$. In particular, the expectations $\mathbb{E}[\tilde{V}^{\varepsilon}_{n,n}(\omega, \tau, z)]$ converge to $\tilde{W}_n(\omega, \tau, z)$, which obey the closed system of transport equations

$$\frac{\partial \tilde{W}_n}{\partial z} + 2n\frac{\partial \tilde{W}_n}{\partial \tau} = \frac{1}{2}\alpha_\beta(\omega)k(\omega)^2 \left((n+1)^2\tilde{W}_{n+1} + n^2\tilde{W}_{n-1} - ((n+1)^2 + n^2)\tilde{W}_n \right),$$
$$\tilde{W}_n(\omega, \tau, z = -L) = \delta(\tau)\mathbf{1}_0(n).$$

We then get the limit of the autocorrelation function of the transmission coefficient:

$$\mathbb{E}\left[T^{\varepsilon}\left(\omega + \frac{\varepsilon^2 h}{2}, -L, 0 \right) \overline{T^{\varepsilon}}\left(\omega - \frac{\varepsilon^2 h}{2}, -L, 0 \right) \right] \overset{\varepsilon \to 0}{\longrightarrow} \int \Lambda^L_{tr}(\omega, \tau) e^{-ih\tau} d\tau, \tag{7.1}$$

$$\Lambda^L_{tr}(\omega, \tau) = k'(\omega)^{-1} \tilde{W}_0(\omega, k'(\omega)^{-1}\tau, 0). \tag{7.2}$$

7.2. Analysis of the transport equations. We can interpret the transport equation in terms of a jump Markov process as in section 6.2. Let us introduce the process $(\tilde{N}_t)_{t \geq 0}$ with state space $\mathbb{N}$ and infinitesimal generator:

$$\tilde{\mathcal{L}}\phi(\tilde{N}) = \frac{1}{2}\alpha_\beta(\omega)k(\omega)^2 \left((\tilde{N}+1)^2(\phi(\tilde{N}+1) - \phi(\tilde{N})) + \tilde{N}^2(\phi(\tilde{N}-1) - \phi(\tilde{N})) \right).$$

Note that $\tilde{\mathcal{L}}$ is the adjoint of the generator $\mathcal{L}$ of the process $(N_t)_{t \geq 0}$, which means that $(\tilde{N}_t)_{t \geq 0}$ is the time reversed process of $(N_t)_{t \geq 0}$. We have

$$\int_{\tau_0}^{\tau_1} \tilde{W}_0(\omega, d\tau, 0) = \tilde{\mathbb{P}}_0 \left(\int_0^L 2\tilde{N}_s ds \in [\tau_0, \tau_1],\ \tilde{N}_L = 0 \right), \tag{7.3}$$

where $\tilde{\mathbb{P}}_{p_0}$ stands for the probability over the distribution of the jump process starting from $\tilde{N}_0 = p_0$. The generating function of the jump process is again expressed in terms of the expectation of some functional of the diffusion process $(\theta_t)_{t \geq 0}$ defined by (6.7):

$$\tilde{\mathbb{E}}_{p_0}\left[z^{\tilde{N}_t} \right] = \mathbb{E}\left[\left(1 - \tanh\left(\frac{\theta_t}{2} \right)^2 \right) \tanh\left(\frac{\theta_t}{2} \right)^{2p_0} \ \middle|\ \theta_0 = 2\ \mathrm{argtanh}(\sqrt{z}) \right].$$

It should be noted also that $\tilde{W}_0$ is not a density with respect to the Lebesgue measure over $\mathbb{R}^+$ (while W_1 is a density, as seen in section 6.2). It consists actually of the sum of a Dirac mass at 0 and a density:

$$\tilde{W}_0(\omega, d\tau, 0) = p_{\omega,d}\delta_0(d\tau) + \tilde{W}_{0,c}(\omega, d\tau, 0).$$

This expression is obtained by disintegrating the right-hand side of (7.3) over the first jump time of the process $(\tilde{N})_{t\geq 0}$. The weight of the Dirac mass is

$$p_{\omega,d} = \exp\left(-\frac{4L}{l_\beta(\omega)}\right),$$

while the absolutely continuous part is given by

$$\int_0^{\tau_1} \tilde{W}_{0,c}(\omega,\tau,0)d\tau = \int_0^L \frac{4}{l_\beta(\omega)} e^{\frac{-4(L-t)}{l_\beta(\omega)}} \tilde{\mathbb{P}}_1\left(\int_0^t 2\tilde{N}_s ds \in [0,\tau_1],\ \tilde{N}_t = 0\right) dt.$$

It seems impossible to derive a closed form expression for the density part. We can either derive expansions or perform numerical simulations based on Monte-Carlo simulations of the random jump process $(\tilde{N}_t)_{t\geq 0}$. For instance, we can expand $\tilde{W}_{0,c}$ for small τ. Indeed, if $\tau_1 \ll l_\beta(\omega)$, then

$$\tilde{\mathbb{P}}_1\left(\int_0^t 2\tilde{N}_s ds \in [0,\tau_1],\ \tilde{N}_t = 0\right) \simeq \frac{2\tau_1}{l_\beta(\omega)} \exp\left(-\frac{4t}{l_\beta(\omega)}\right),$$

so that

$$\tilde{W}_{0,c}(\omega,\tau,0) \overset{\tau \ll l_\beta(\omega)}{\simeq} \exp\left(-\frac{4L}{l_\beta(\omega)}\right) \frac{8L}{l_\beta(\omega)^2}.$$

This approximate expression will be used in the next section to give a closed form expression of the refocused pulse in a particular regime.

7.3. The refocused pulse. The following theorem expresses the self-averaging property of the refocused pulse.

THEOREM 7.1. *For any $T > 0$, $\delta > 0$,*

$$\mathbb{P}\left(\sup_{t\in[-T,T]} \left|\eta^\varepsilon_{tr(TRT)}\left(\frac{t_1+L}{\varepsilon^2} + t, z = 0\right) - \eta_{tr(TRT)}(t)\right| > \delta\right) \overset{\varepsilon\to 0}{\longrightarrow} 0,$$

where $\eta_{tr(TRT)}$ is the refocused pulse shape:

$$\eta_{tr(TRT)}(t) = \left(f(-\,\cdot) * K_{TRT}(\cdot)\right)(t). \tag{7.4}$$

The Fourier transform of the kernel is the convolution of the time-inverted cut-off function G_{t_0,t_1} with the density $\tau \mapsto \Lambda^L_{tr}(\omega,\tau)$ evaluated at $(1-k'(\omega))L$:

$$\begin{aligned}\hat{K}_{TRT}(\omega) &= \left(G_{t_0,t_1}(-\,\cdot) * \Lambda^L_{tr}(\omega,\cdot)\right)((1-k'(\omega))L) \\ &= \int G_{t_0,t_1}(\tau - (1-k'(\omega))L)\Lambda^L_{tr}(\omega,d\tau).\end{aligned} \tag{7.5}$$

Proof. The proof follows the same lines as that of Theorem 6.1 with the transport equations corresponding to the transmission problem. ∎

Homogeneous dispersive case. Assume here that randomness is absent ($\alpha_\beta(\omega) \equiv 0$). Then $\Lambda^L_{tr}(\omega,\tau) = \delta_0(\tau)$, so that

$$\hat{K}_{TRT}(\omega) = G_{t_0,t_1}((k'(\omega)-1)L),$$

which is consistent with the results of section 5.4 at $z = 0$.

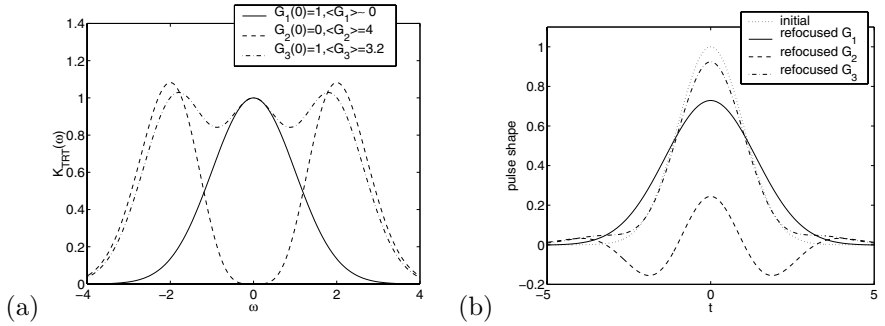

FIG. 7.1. *Fourier transform of the convolution kernel* K_{TRT} (a) *and refocused pulse* (b). *We consider the three cut-off functions* G_1, G_2, G_3 *described within the text. Here we assume* $\alpha(\omega) \equiv 1$, $L = 1$. *The initial pulse has Gaussian shape* $f(t) = \exp(-t^2/2)$.

Random nondispersive case. Assume here that $\beta = 0$. Consider an input pulse f which is such that the power spectral density of the process m can be considered as constant over the spectral range $[-\omega_{max}, \omega_{max}]$ of f: $\alpha(\omega) \equiv \alpha_0$. Finally, assume that we record a small piece of the transmitted wave in the sense that the cut-off function G_{t_0,t_1} has its support in $[t_0, t_1]$ such that $t_0 < 0$ and $t_1 > 0$ with $\alpha_0 \omega_{max}^2 t_1 \ll 1$. Then

$$\hat{K}_{TRT}(\omega) = e^{-\frac{\alpha_0 \omega^2 L}{2}} \left(G_{t_0,t_1}(0) + \frac{\alpha_0^2 \omega^4 L}{8} \langle G_{t_0,t_1} \rangle \right),$$

where $\langle G_{t_0,t_1} \rangle = \int_0^\infty G_{t_0,t_1}(t)dt$, so that

$$\eta_{tr(TRT)}(t) = G_{t_0,t_1}(0) \left(f(-\,\cdot) * K_{TRT,1}(\cdot) \right)(t) + \langle G_{t_0,t_1} \rangle \left(f(-\,\cdot) * K_{TRT,2}(\cdot) \right)(t),$$

$$\hat{K}_{TRT,1}(\omega) = e^{-\frac{\alpha_0 \omega^2 L}{2}},$$

$$\hat{K}_{TRT,2}(\omega) = \frac{\alpha_0^2 \omega^4 L}{8} e^{-\frac{\alpha_0 \omega^2 L}{2}}.$$

The convolution kernel $K_{TRT,1}$ results from the double action of the O'Doherty–Anstey theory on the front pulse in forward and backward directions. Of course this contribution completely vanishes if we do not record the front of the pulse ($G_{t_0,t_1}(0) = 0$). The convolution kernel $K_{TRT,2}$ is a filter that retains only the frequencies around $1/\sqrt{\alpha_0 L}$, those which can probe the medium without being completely reflected by the strong localization effect.

7.4. Numerical illustrations. We would like to illustrate results obtained in the previous section. We consider the hyperbolic random case discussed in subsection 7.3. In Figure 7.1 we plot the Fourier transform of the kernel K_{TRT} for three different time reversal calculations corresponding to three different cut-off functions G_{t_0,t_1} that we shall denote by G_1, G_2, and G_3. In the first calculation, we record only the front pulse and send it back into the medium $G_1(0) = 1$, $\langle G_1 \rangle \ll L$. We may think, for instance, that

$$G_1(t) = \cos^2\left(\frac{t}{t_1}\right) \mathbf{1}_{[-\pi t_1/2, \pi t_1/2]}(t),$$

with $\alpha_0 \omega_{max}^2 t_1 \ll 1$ and $t_1 \ll L$. The refocused pulse results from the action of the O'Doherty–Anstey theory, and its shape is the convolution of the initial pulse shape with the kernel $K_{TRT,1}$ (solid line, Figure 7.1).

In the second calculation, we record a small piece of the coda but not the front pulse $G_2(0) = 0$, $\langle G_2 \rangle = 4L$. We may think, for instance, that

$$G_2(t) = \frac{8L}{\pi t_1} \sin^2\left(\frac{t}{t_1}\right) \mathbf{1}_{[0,\pi t_1]}(t),$$

with $\alpha_0 \omega_{max}^2 t_1 \simeq 0.1 - 0.2$. Only medium range frequencies have been recorded, so that the refocused pulse shape is the convolution of the initial pulse shape with the kernel $K_{TRT,2}$ (dashed line, Figure 7.1).

In the third calculation, we record both the front pulse and a piece of the coda, so that $G_3(0) = 1$, $\langle G_3 \rangle \simeq 3.2L$. We may think, for instance, that

$$G_3(t) = \frac{6.4L}{\pi t_1} \sin^2\left(\frac{t + t_0}{t_1}\right) \mathbf{1}_{[-\pi t_0, \pi(t_1 - t_0)]}(t),$$

with $\alpha_0 \omega_{max}^2 t_1 \simeq 0.1 - 0.2$ and $t_0 \simeq \sqrt{\pi t_1^3/(6.4L)}$. In such a case a broad range of frequencies are recorded, and the cut-off function has been chosen in such a way that the weighted sum of the two kernels $K_{TRT,1}$ and $K_{TRT,2}$ define a kernel K_{TRT} with a large band of frequencies (dash-dotted line, Figure 7.1). As a result, the refocused pulse is close to the initial pulse.

It has been observed experimentally [10] that retransmitting part of the coda produces better refocusing than resending the front. This observation addresses spatial refocusing, while in this paper we focus our attention on time refocusing. The above illustrations show that the contributions of the coda and the front to the refocused pulse are actually complimentary. The contribution of the front is concerned with the low-frequency components of the pulse, while the contribution of the coda is concerned with the high-frequency components of the pulse. If we extrapolate this observation to three-dimensional configurations, then we can understand the quoted experimental observation in the sense that the high-frequency components are the ones that are expected to give the precise location of the source point.

7.5. TRT numerical experiments and application to source reconstruction. In this section we further illustrate TRT. A numerical method for the nonlinear terrain-following Boussinesq equation has been fully described in [19]. In this section we describe time reversal experiments in transmission by performing numerical experiments corresponding to the linearized terrain-following Boussinesq system (2.1)–(2.2). The initial wave elevation profile is incoming from the left and is given either by a Gaussian $\eta_0(z) = f(z) = \exp(-z^2/0.05)$ or by its spatial derivative $f'(z)$, as displayed in Figure 7.2. The corresponding initial velocity field is calculated in order to generate only a right-propagating mode, as presented in section 3. This is easily done by performing the inverse FFT of $\check{u} \equiv (\omega/k)\check{f}$.

7.5.1. Previous numerical results in related configurations. In a previous article by Fouque and Nachbin [15], TRR numerical experiments were conducted with a weakly nonlinear shallow water system. In particular, formula (6.10) (for the refocused pulse shape in reflection) was numerically captured in the hyperbolic ($\beta = 0$) case. The corresponding formula in [15] reads as (6.10) with K_{TRR}, as given by expression (6.13), with $\kappa_{(\beta=0)}(\omega) = \alpha(\omega)/4$. A weakly nonlinear example was also presented showing that formula (6.10) with $\beta = 0$ still holds as a good approximation. As a consequence of these early results, a complete nonlinear hyperbolic theory has been recently developed by the present authors [13]. Subsequently [14, 19] nonlinear

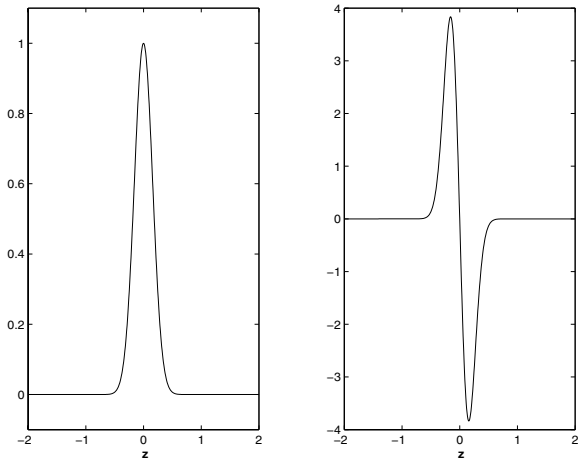

FIG. 7.2. *Initial wave elevation profiles considered in the experiments.*

experiments were further extended, and several numerical experiments for TRR were presented for both linear and weakly nonlinear dispersive waves, including solitary waves. Theory is not yet available for weakly dispersive, weakly nonlinear (solitary) waves.

Connecting the above comments and previous results with the present paper, we recall that numerical results for the transmitted front (as at the end of section 5.2) were presented by Grajales and Nachbin in [18]. The present numerical code captured quantitatively the composition of both kernels K_d and K_r, defined through (5.6). One should keep in mind that the present stochastic O'Doherty–Anstey formulation in transmission is more general than the deterministic theory given in [18], in part because it does not necessarily rely on β being small and also because it displays the *self-averaging* property. Moreover, time reversal was not addressed in [18].

Hence it is important to note that the transmission formula (5.6) plays an essential role in expression (5.7), which converges asymptotically to the TRT formula (7.4). The limiting form (7.1) of the frequency autocorrelation function was studied in section 7.1 and is characterized by the solution $\tilde{W}_0$ of a transport equation, as indicated in (7.2). In contrast to the TRR problem it is not possible to derive a closed form expression for the power spectral density Λ^L_{tr}, as mentioned at the end of section 7.2. One can derive expansions or perform Monte-Carlo simulations with the corresponding jump process. On the other hand, in the TRR problem this was made possible with the large slab hypothesis (section 6.4), leading to a closed form expression for Λ^∞_{ref}. Thus extracting quantitative information from expression (7.4) is a complex task, particularly due to the difficulty of computing Λ^L_{tr}.

Our strategy for presenting numerical results that address the theoretical expression for TRT is as follows. In section 7.3 a dispersive regime was identified where TRT can be easily checked: the homogeneous dispersive case. It has never been verified that the oscillatory effect of the Airy kernel can be completely recompressed, even for large values of β where we end up completely losing track of the initial pulse shape. Phases are scrambled due to dispersion but recompressed (reorganized) through time reversal. This will be shown below.

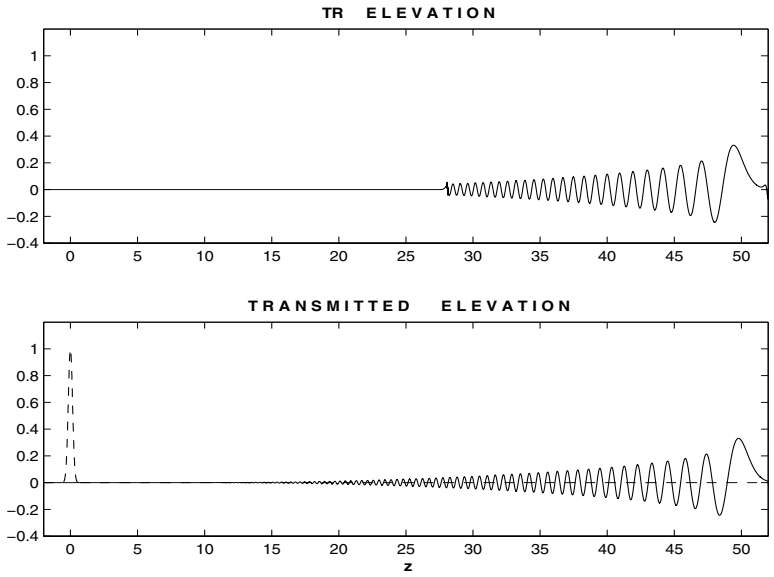

FIG. 7.3. *Bottom graph: the complete transmitted wave elevation. The initial condition is given by a dashed line. Dispersive propagation ($\beta = 0.01$) over a flat bottom. Top graph: cut-off wave elevation profile to be time reversed and sent back towards the origin.*

The next step is to add randomness. In forward transmission the dispersive O'Doherty–Anstey attenuation mechanism has been quantitatively validated in [18], for a specific realization. Note that these are two separate ways of addressing the two main mechanisms encoded in Λ_{tr}^{L}: the dispersive and the incoherent coda production and recompression. Finally, in the absence of a closed form expression for Λ_{tr}^{L}, we proceed to qualitatively verifying the combined effect for the dispersive TRT in a random environment.

7.5.2. New experiments for dispersive TRT. The new experiments of interest are in the TRT regime illustrating how, in particular, it can be applied to source reconstruction (i.e., waveform inversion).

We first consider the homogeneous dispersive case discussed above. In this problem a Gaussian pulse will be gradually transformed into an Airy function (cf. section 5.4, case (b)). An oscillatory tail develops behind the wavefront due to dispersion, as displayed in Figure 7.3. TRT will recompress the oscillatory tail, and the initial waveform is obtained as indicated in the sequence of Figure 7.4. In these experiments we used the Gaussian pulse (of approximately unit width) for the right-propagating initial elevation, together with its consistent (right-going) dispersive velocity profile ($\beta = 0.01$). Both the wave elevation η and the wave velocity u were recorded for time reversion. Hence no right-going mode was produced in the time reversed experiment.

Dispersion is then increased to a level where we will completely lose track of the initial pulse shape. Let $\beta = 0.1$, and consider the derivative of a Gaussian for the initial profile $\eta_0(z)$. In Figure 7.5 we present the forward experiment (in the top graph), having only a right-going mode. Time evolves from bottom trace to the top. The final trace (at the top) shows that we have completely lost track of the initial profile highlighted in the bottom trace. Both η and u are recorded and time reversed. Hence

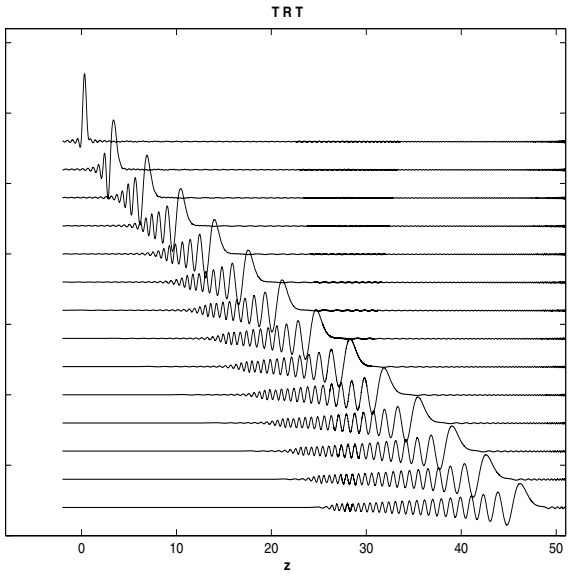

FIG. 7.4. *Time reversal in transmission (TRT) over a flat bottom. The initial profile was a Gaussian at the origin. The time reversed profile is the trace at the bottom. Time evolves from bottom to top at time increments of* 3.6 *units. Complete refocusing is observed in the top trace. The dispersion level is* $\beta = 0.01$.

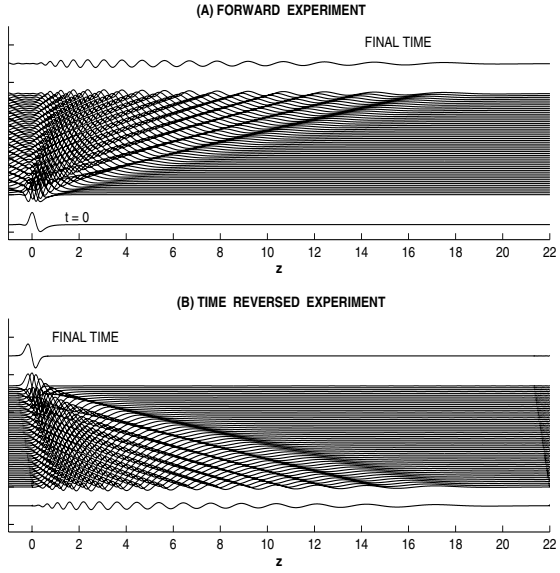

FIG. 7.5. *TRT over a flat bottom. The initial profile is a derivative of a Gaussian at the origin (bottom trace of graph* (A)*). Time evolves from bottom to top. Full recompression is observed in graph* (B). *The dispersion level has been increased to* $\beta = 0.1$.

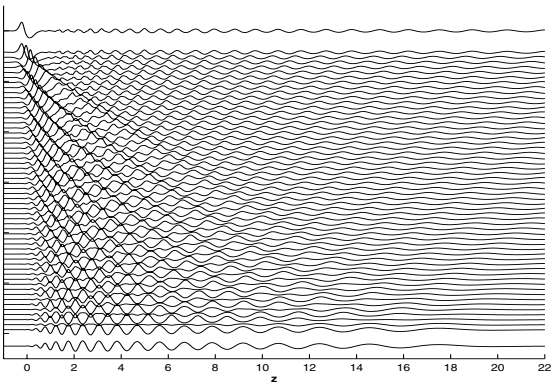

FIG. 7.6. *TRT over a flat bottom. Time evolves from bottom to top. The TR wave elevation (bottom trace) was amplified by a factor of two, while the velocity field u was not used for TR.*

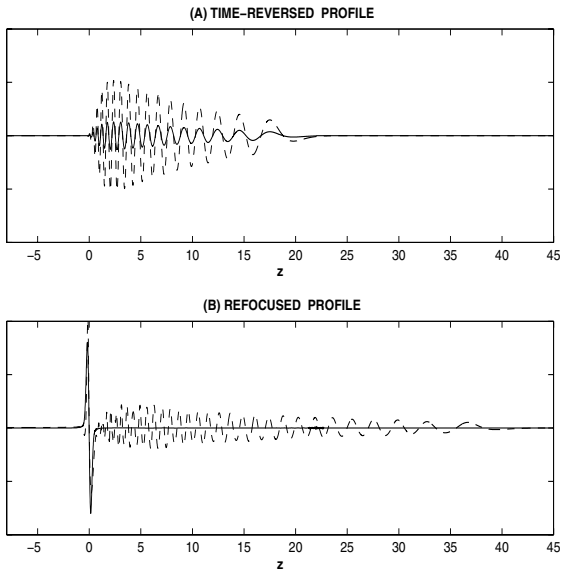

FIG. 7.7. (A) *Solid line: the recorded η; dashed line: the amplified η for time reversion.* (B) *Refocused pulse for the amplified experiment of Figure* 7.6 *(dashed line) and for the experiment in Figure* 7.5 *(solid line).*

a left-propagating mode is generated for the time reversed experiment. In the bottom graph of Figure 7.5 we clearly see the full recompression as predicted in section 5.4.

Next we consider the case where we record only the wave elevation η. For the time reversal experiment we re-emit this elevation field with a two-fold amplification. The corresponding dynamics is presented in Figure 7.6. We clearly see that, as recompression takes place along the left-propagating mode, there is a small dispersive wave propagating to the right. In Figure 7.7(A) we have the "doubled" time reversed profile compared to the recorded profile. In Figure 7.7(B) we see that the refocused pulse is the same for both experiments considered with $\beta = 0.1$. The oscillatory coda seen in

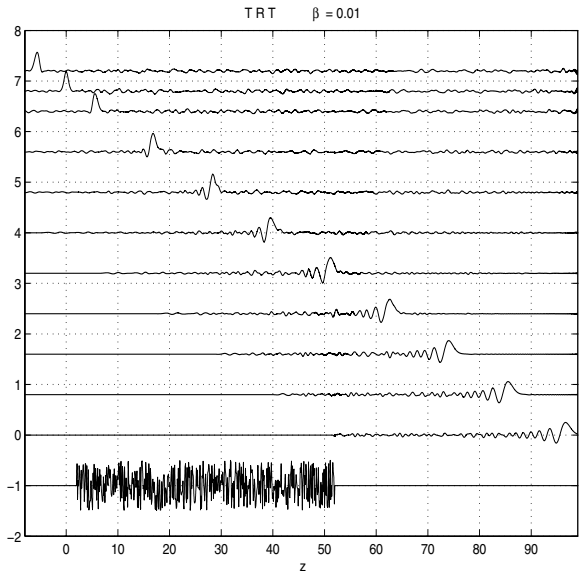

FIG. 7.8. *TRT over a random topography. The fluctuation level is* 50% *and the correlation length is* $\varepsilon = 0.1$. *The realization of the topography used for the simulation is given at the bottom. Just above the topography we have the wave elevation profile used for time reversion. Then time evolves from bottom to top in increments of* 11.52 *time units. The expected refocusing time takes place at half the time increment used and is therefore graphed accordingly.*

Figure 7.7(B) is due to the right-propagating mode in the "amplified" experiment.

We now repeat both TRT experiments in the presence of a random topography expressed through the coefficient $M(z)$. In these experiments both η and u are used in the time reversed data. In Figure 7.8 a realization of the random topography is given at the bottom of the graph, together with the transmitted wave elevation which will be time reversed and sent back into the random medium. Note that to the left of the (transmitted) oscillatory coda we have (small) incoherent radiation. At the correct time the deterministic front, coda, and random radiation recompress to give rise to (a reduced version of) the original waveform, namely a Gaussian. The correct time is exactly the time for the wave to reach the origin ($t = 97.92$). This was the time up to which the time reversed signal was originally recorded. Note, however, that the resolution of the source location is rather poor. The three upper curves in Figure 7.8 show almost the same waveform. This is of course an expected consequence of the hyperbolicity of the equations.

Our final illustration of TRT considers strong dispersive effects. In the previous example we had $\beta = 0.01$. Now we consider a value ten times larger. We now adopt the Gaussian's derivative as the initial wave elevation profile. This function has more energy on higher Fourier modes than the Gaussian. Thus the effect of dispersion will be even more noticeable. In Figure 7.9 we see the topography realization at the very bottom of the figure. Above the topography we find the transmitted wave elevation profile to be used in the time reversal experiment. This profile was recorded after 95.4 time units. The corresponding velocity profile is reversed. From bottom to top, the next three curves correspond to times $t = 91.8, 95.4$ (the expected refocusing time), and 99 time units. Only at time $t = 95.4$ do we have the original initial profile. At neigh-

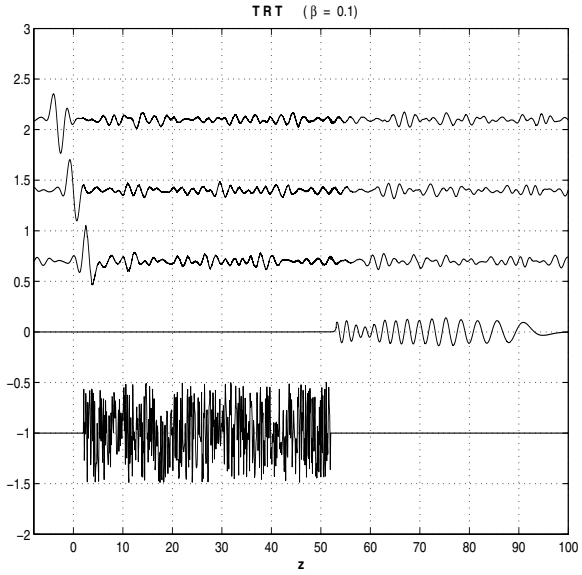

FIG. 7.9. *TRT over a random topography. The dispersion level has been increased* 10 *times* ($\beta = 0.1$). *The trace at the bottom represents the time reversed wave elevation profile. The three following curves (from bottom to top) correspond to times* $t = 91.8$, 95.4 *(the expected refocusing time), and* 99 *time units. The topography's fluctuation level is* 50%, *and the correlation length is* $\varepsilon = 0.1$.

boring times we see the effect of dispersion. At $t = 91.8$ we see that the oscillatory coda (here ahead of the left-propagating pulse) is still being recompressed. At time $t = 99$ the pulse starts developing the usual dispersive coda behind it. The wave source is located at the origin with a much higher accuracy than in the hyperbolic case. The source location is precisely the point between coda recompression and coda generation. Note that from the TR initial profile (at the bottom of Figure 7.9) it is very difficult to predict the source's waveform, while TRT has naturally performed the waveform inversion. We are currently working on the extension of these results and applications to higher dimensions. A good numerical model and bathymetric information can be invaluable tools for performing the time reversed dynamics and waveform inversion.

8. Conclusion. In this paper we have addressed the time reversal for waves governed by a random dispersive Boussinesq system. We have demonstrated that source location by time reversal is more effective in the dispersive case than in the hyperbolic case, because the source location is precisely the point between coda recompression and coda generation. Our analysis also shows that dispersion enhances localization effects in random medium. As a result, time reversal focusing in reflection (resp., in transmission) is more efficient (resp., less efficient) in the dispersive case than in the hyperbolic case, as indicated in Figure 6.1(a). Extension to more general dispersion relations is straightforward. The only but important hypothesis is that the addressed dispersion relation $k(\omega)$ should be an odd function so that it preserves time reversibility. These statements can also be generalized to some extent to three-dimensional configurations. In 3D configurations the pulse refocuses in time and in space [12, 6]. Accordingly, even in absence of dispersion source localization is possible, as it is given

by the point where the refocused wave reaches its climax. However, we conjecture that dispersion improves the resolution of the source location, as the pulse spreading is enhanced when propagating away from the original source location. Furthermore, the spectral phase modulations are larger in the presence of dispersion, so that only close wavenumbers are phase-matched. We can thus expect that dispersion enhances the statistical stability as well as the super-resolution in spatial refocusing described in [3, 6, 23], and in time refocusing as described in this paper.

REFERENCES

[1] M. Abramowitz and I. Stegun, *Handbook of Mathematical Functions*, Dover, New York, 1965.

[2] M. Asch, W. Kohler, G. Papanicolaou, M. Postel, and B. White, *Frequency content of randomly scattered signals*, SIAM Rev., 33 (1991), pp. 519–625.

[3] G. Bal, G. Papanicolaou, and L. Ryzhik, *Self-averaging in time reversal for the parabolic wave equation*, Stoch. Dyn., 2 (2002), pp. 507–531.

[4] G. Bal, T. Tomorowski, and L. Ryzhik, *Self-averaging of Wigner transforms in random media*, Comm. Math. Phys., 242 (2003), pp. 81–135.

[5] G. Bal and L. Ryzhik, *Time reversal and refocusing in random media*, SIAM J. Appl. Math., 63 (2003), pp. 1475–1498.

[6] P. Blomgren, G. Papanicolaou, and H. Zhao, *Super-resolution in time-reversal acoustics*, J. Acoust. Soc. Am., 111 (2002), pp. 230–248.

[7] R. Burridge, G. Papanicolaou, and B. White, *Statistics for pulse reflection from a randomly layered medium*, SIAM J. Appl. Math., 47 (1987), pp. 146–168.

[8] J. F. Clouet and J. P. Fouque, *Spreading of a pulse traveling in random media*, Ann. Appl. Probab., 4 (1994), pp. 1083–1097.

[9] J. F. Clouet and J. P. Fouque, *A time-reversal method for an acoustical pulse propagating in randomly layered media*, Wave Motion, 25 (1997), pp. 361–368.

[10] A. Derode, P. Roux, and M. Fink, *Robust acoustic time reversal with high-order multiple scattering*, Phys. Rev. Lett., 75 (1995), pp. 4206–4209.

[11] M. Fink, *Time reversal mirrors*, J. Phys. D: Appl. Phys., 26 (1993), pp. 1333–1350.

[12] M. Fink, *Time reversed acoustics*, Scientific American, November (1999), pp. 91–97.

[13] J.-P. Fouque, J. Garnier, and A. Nachbin, *Shock structure due to stochastic forcing and the time reversal of nonlinear waves*, Phys. D., to appear.

[14] J.-P. Fouque, J. Garnier, J. C. Muñoz Grajales, and A. Nachbin, *Time reversing solitary waves*, Phys. Rev. Lett, 92 (2004), paper 094502.

[15] J.-P. Fouque and A. Nachbin, *Time-reversed refocusing of surface water waves*, Multiscale Model. Simul., 1 (2003), pp. 609–629.

[16] J.-P. Fouque and K. Solna, *Time-reversal aperture enhancement*, Multiscale Model. Simul., 1 (2003), pp. 239–259.

[17] P. Lewicki, R. Burridge, and G. Papanicolaou, *Pulse stabilization in a strongly heterogeneous medium*, Wave Motion, 20 (1994), pp. 177–195.

[18] J. C. Muñoz Grajales and A. Nachbin, *Dispersive wave attenuation due to orographic forcing*, SIAM J. Appl. Math., to appear.

[19] J. C. Muñoz Grajales and A. Nachbin, *Stiff microscale forcing and solitary wave refocusing*, Multiscale Model. Simul., to appear.

[20] A. Nachbin, *A terrain-following Boussinesq system*, SIAM J. Appl. Math., 63 (2003), pp. 905–922.

[21] G. C. Papanicolaou, *Wave propagation in a one-dimensional random medium*, SIAM J. Appl. Math., 21 (1971), pp. 13–18.

[22] G. Papanicolaou, *Asymptotic analysis of stochastic equations*, in MAA Stud. in Math. 18, M. Rosenblatt, ed., Mathematical Association of America, Washington, DC, 1978, pp. 111–179.

[23] G. Papanicolaou, L. Ryzhik, and K. Solna, *Statistical stability in time reversal*, SIAM J. Appl. Math., to appear.

[24] C. Pires and P. M. A. Miranda, *Tsunami waveform inversion by adjoint methods*, J. Geophys. Res., 106 (2001), pp. 19773–19796.

[25] K. Solna and G. Papanicolaou, *Ray theory for a locally layered medium*, Waves in Random Media, 10 (2000), pp. 151–198.